ABSTRACT

YOUNG, ERIC STEPHEN. Ultrasound-Based Biomedical Implantable Device. (Under the direction of Dr. Ömer Oralkan and Dr. George Ligler).

A diverse set of stimulators, transducers and data transceivers can be integrated into medically implantable devices using ultrasonic power. An application for such a device is postoperative monitoring of abdominal aortic aneurysm repair. Endoleaks are a potentially serious, but correctible, complication of aorta repair. A miniscule ultrasonic powered device incorporated into the stent-graft for endovascular delivery could provide on demand diagnostic information about the presence of endoleak by monitoring the dimensions of the aneurysm sack and/or stent-graft in real time. In this work, a wireless ultrasonic power recovery scheme is demonstrated in oil using a single-element capacitive micromachined ultrasonic transducer, and a circuit made with commercially off-the-shelf discrete components. The 2-mm diameter CMUT element, a diode rectifier bridge and inductor-based boost circuit form the power conversion circuit delivering over 1 mW to the load. Other aspects of the implantable device that have been demonstrated are a pulse echo measurement of the diameter of the endovascular aneurysm repair device lumen, and a data transmission method that encodes clock, data and transmission framing information in biphasic ultrasonic pulses and takes advantage of the wideband characteristics of the CMUT. This proof of concept is guiding the design of an integrated circuit implementing the key elements of the implantable device: wireless power, data uplink and clinical measurement. For a compact solution and to facilitate translation, the integrated circuit version will accomplish these three functions using a single, shared CMUT device.

Ultrasound-Based Biomedical Implantable Device

by
Eric Stephen Young

A thesis submitted to the Graduate Faculty of
North Carolina State University
in partial fulfillment of the
requirements for the degree of
Master of Science

Biomedical Engineering

Raleigh, North Carolina
2020

APPROVED BY:

_____	_____
Ömer Oralkan Committee Co-Chair	George Ligler Committee Co-Chair
_____	_____
David Lalush	Frances Ligler

DEDICATION

I started the pursuit of this degree, and this research topic, to make an impact on healthcare - leveraging 25 years of industry experience in electronics, integrated circuit design and engineering. The combination of medicine with engineering is for me the fusion of my upbringing among the medical community which dominated the first half of my life, and the mature years of my life spent in a career applying electronics technology to provide solutions in consumer, automotive and industrial applications. I hope the tiny contribution described in this thesis will improve accessibility, cost and clinical outcomes in healthcare.

I would like to dedicate this work to my family: that is to my parents (Dr. Stephen Young, and Dr. Margaret Young), wife (Melinda) and children (Zachary, Benjamin, Marie, Isaac and Hannah). Thank you all for giving me the inspiration to leverage the present to fuse the future (yours and mine) with the past; and hopefully my work will be relevant for years to come in a rapidly changing world.

Soli Deo Gloria.

BIOGRAPHY

Eric Young was born in Galveston, TX in 1968. His parents were medical doctors, so he grew up around the medical college and around patient care in the days when children could tag along with their parents on rounds or procedures. After earning a BS in Nuclear Engineering at Purdue University he worked for the Department of Energy as a headquarters-based engineer for the nuclear and accelerator facilities used to certify electronics for exposure to harsh radiation environments. Motivated by the opportunities he saw in electronics, he returned to graduate school at University of Maryland in electrical engineering in 1995. Eric married Melinda in 1996, finished the MS degree and saw the birth of their first child in 1997. In 20 years of industry work at Atmel, Motorola, Maxim and Linear Technology he has contributed to the heady early days of field programmable gate arrays, automotive airbag deployment systems, cellphone power management circuits, general purpose switch-mode circuits for DC-DC power conversion, and automotive/industrial LED drivers. During those years, Eric and Melinda have had five more children, and have resided for the majority of that time in Apex, NC. In late 2017, after the close of the purchase of the company he worked for, Linear Technology, by Analog Devices, Eric decided it was a good opportunity to return to school to broaden his horizons beyond switch-mode power to include many new technologies, with a focus on healthcare. He was admitted to the UNC-NCSU Joint Department of Biomedical Engineering starting in August 2018. He accepted an engineering position in industry at Analog Devices, starting in December 2019.

ACKNOWLEDGMENTS

I would like to acknowledge my research advisor, Dr. Ömer Oralkan, for supporting my application to the graduate school in UNC-NCSU Joint Department of Biomedical Engineering, and for taking on my unique case by sponsoring this research in his group as a Research Assistant. The application idea he paired me with leveraged my experience with power conversion and circuits, and allowed me to exercise my newly gained knowledge in ultrasonics and biomedical electronics. I appreciate that my assignments in the IMIST group, and even before joining the graduate program, as a student in his class on MEMS devices, have allowed steady progress towards the goal of demonstrating this implantable device concept that uses capacitive machined ultrasonic transducers. Thanks also to the graduate and postdocs in the IMIST group who helped me with the lab software and setting up experiments, including Dr. F. Yalcin Yamaner, Jeanne Sanders, Marzana Mahmud, Chunkyun Seok, and Ali Onder Biliroglu.

This work was supported by the National Science Foundation under Grant 1160483 as part of a Center-to-Centre collaborative partnership with NUI Galway, Ireland and Queens University, Belfast, Northern Ireland. I would like to recognize Sean Cummins from NUI Galway for the advice he provided based on his role in mechanical design of the delivery system, and translational studies. The project is administered by the ASSIST center, with Michael Daniele as overall principal investigator. Dr. Daniele defined the second use of the wireless implantable, for monitoring ingrafting of an engineered tissue patch for cardiac muscle regeneration. Without the seed ideas motivating it, and collaboration of the team members, I feel this work would have been relegated to novelty instead of enabling technology. Thanks to our industry partner, Cook Medical for providing the EVAR samples used to investigate the pulse-echo ranging capability and characteristics.

I would also like to acknowledge the professors who have contributed to the improvement of my knowledge base with their courses which I attended: Michael Gamcsik, David Lalush, Greg Trahey, Elaine Bohorquez, Brian Floyd, David Ricketts, and Yaoyao Jia.

Without the encouragement and cameraderie of my fellow biomedical engineering PhD students from the class of 2018, inside and outside of the classroom, this would have been a much more difficult and lonely endeavor. I hope to continue working with them in the future; regardless of the outcome with this work, I wish them the best in all their endeavors.

Finally, I could not have done this career re-tooling without the loving support of my wife, Melinda. She kept the family running while I worked weekends and nights on the research and coursework. This uncommon experiment involving breaking off mid-career to pursue graduate studies, was conducted under the watchful eyes of my children, some of whom wish to pursue a career in medicine or engineering. It was also observed by my colleagues in industry through my "blog". I hope these folks can take away some encouragement about biomedical engineering, and the possibility of chasing new dreams as an older adult.

TABLE OF CONTENTS

LIST OF FIGURES

CHAPTER 1. Introduction

1.1 Motivation

This work describes proof-of-concept studies for using ultrasound to implement the three primary functions of a wireless biomedical implantable device: power, communication, and measurement or therapy. These three functions were demonstrated in isolation from each other, but with an integrated circuit electronic device they could be combined into a powerful platform for biomedical monitoring. Using micromachining technology for the transducer and industrial-scale silicon electronic device technology for the integrated circuit, it is possible to achieve a tiny heterogeneously integrated device that can be delivered by catheter deep into the tissues to fulfill some unmet needs in biomedical monitoring and/or therapy. Two potential use cases are presented involving performance monitoring of tissue grafts, but this is by no means the limit.

Miniscule micropower electronic devices based on ultrasonic technology are ideal for biomonitoring and bio-stimulation applications which require a very small form factor. Ultrasound is a proven and a powerful tool to measure key parameters of interest, i.e., distances, pressures and flows, in various challenging environments. This rich body of diagnostic information is enabled by the unique characteristics of its coherent energy: the millimeter wavelengths provide excellent spatial resolution; and the relatively slow propagation speeds allow electronics and transducers to shape the waveform of the emitted ultrasonic energy and to record the received energy (usually reflected from a target or tissue interface) in real time. This ability to capture the phase, frequency and amplitude of the ultrasonic energy allows the use of powerful signal processing tools to produce images or make distance vs. time measurements at a physical resolution that is not possible using electromagnetic energy.

Ultrasonic wireless power transfer can supply implants much deeper in biological tissue compared to alternative sources using inductive coupling or radio frequency (RF). Ultrasound enjoys a comparative advantage over RF in regards to miniaturization of the receiver and focusing of the energy because ultrasound energy wavelength is five orders of magnitude smaller at a given frequency. Inductive coupling is powerful but is practically limited to a couple centimeters range in tissue due to limited size for the implantable receiver coils [1] [2] [3]. The 7.2 mW/mm^2 safety limit for acoustic power exposure in diagnostic imaging, coupled with a reasonably efficient acoustic to electrical converter, is sufficient to supply various loads in either pulsed or continuous modes, with the pulsed mode being of particular interest for monitoring applications with data uplink. Miniscule motes, deliverable by catheter, having limited energy storage capability and energizing transiently in response to absorption of ultrasonic energy, will excel in applications where deeply embedded devices are polled or activated infrequently with long intervals of dormancy.

Ultrasound applications stand to benefit from expansion of micromachined electro-mechanical system (MEMS) technology that has continuously improved since its beginnings almost 40 years ago [4]. The piezoelectric technology which has been the mainstay for ultrasonic transducers for the past 100 years, is now supplemented within the past couple decades by a MEMS technology called the capacitive micromachined ultrasonic transducer (CMUT) [5]. The new CMUT device boasts advantages in manufacturability, integration and performance. The technology to manufacture the CMUT is based on the silicon technology used to make commercial electronics, which has experienced at least five decades of continuous improvements in device size, yield, and cost. The compact integration of CMUT transducers

with supporting electronic circuits is critical for efficacy of the overall system, and it is possible in large part because they share the same basic technology.

The primary limitations encountered with ultrasound systems for imaging and diagnostics come from the electronics and how they interface to the transducers that transmit and receive the ultrasound. As stated previously, the electronics are able to record the ultrasonic waveforms with high fidelity, but this capability produces tremendous amounts of data to be manipulated. The closer the electronics are placed to the transducer, the better quality is the data, and the more compact is the solution. Fortunately, the ever present need to increase transistor density to pack more functions into a smaller space has been satisfied by steady improvements in technology. Moore's law observes that the number of transistors has doubled every two years for the past 50 years [6]. As size decreases, power also decreases, especially for circuits using complementary metal-oxide silicon (CMOS) transistor devices. An important companion technology to CMOS are the bipolar transistors. These are very useful for low-offset low-noise circuits such as amplifiers and reference generators, and for circuits that run from either very high or very low voltages. Industry processes combining the two types of devices, bipolar and sub-micron CMOS (i.e., BiCMOS), are available to the university community for designing biomedical applications [7]. New opportunities for ultrasonic technology, such as the one described in this thesis, emerge with improvements to electronics and transducer technology.

Wirelessly powered ultrasonic devices are already in use in critical biomedical applications. A wireless cardiac stimulator (WiCS) device for cardiac resynchronization therapy, powered by ultrasonic energy, has been in development by EBR Systems since 2011 [8]. This device was recently approved by the FDA for patient use. The WiCS device solves a problem with pacing the left ventricle of the heart – previously a leaded electrode had to puncture the

septal wall to deliver the resynchronizing pulses to the correct location. EBR Systems WiCS stimulator electrode is implanted in the left ventricle with no lead. It receives its ultrasonic energy in a 9 mm by 2.5 mm piezoelectric transducer and delivers the resynchronization pulse to heart muscle. The electronics of this implant are not sophisticated, but WiCS is a good example of innovation in the implantable medical device application space.

A different miniaturized ultrasonic implantable device is developed by a team at UC Berkeley for neural monitoring and stimulation. [9] [10]. This "neural dust" is powered wirelessly by ultrasonic energy and communicates by modulating the acoustic properties of the device. The transducer in this research uses piezoelectric technology, but it is not difficult to imagine that CMUT technology would provide a thinner aspect ratio improving delivery and biocompatibility.

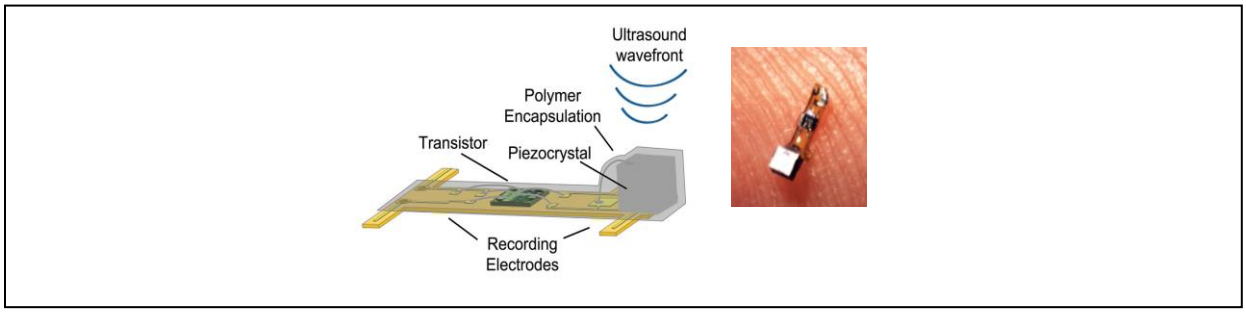

Figure 1. "Neural Dust" uses piezoelectric based ultrasonic power harvesting for neural recording.

The application for an ultrasonically powered implantable device presented in this thesis work is postoperative monitoring of abdominal aortic aneurysm (AAA) repair. AAA is present in as much as 7.6% of the male population ages 65 to 80 years old, and a lower percentage of the female population. Approximately 1.7 million individuals in the United States (USA) alone are afflicted. An epidemiology study in the USA suggests more than 40,000 AAA repair procedures are performed every year, most elective/preventive but some due to acute rupture. The mortality rate for ruptured AAA is greater than 50% [11]. Most of the repair procedures (75%) use endo-vascular aneurysm repair (EVAR) stent-graft devices delivered by catheter as shown in figure 2.

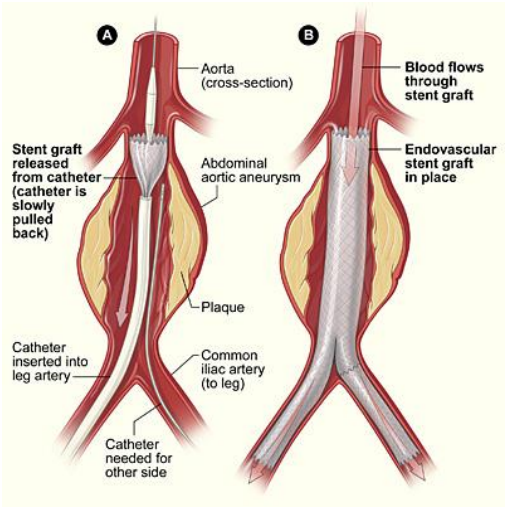

Figure 2. EVAR Procedure showing deployment of stent by catheter. Source: https://surgery.ucsf.edu/conditions-procedures/endovascular-aneurysm-repair.aspx

Endoleaks are a potentially serious, but correctible, long-term complication of the EVAR procedure. The gold standard for detection of endoleak is contrast dye enhanced computed tomography or magnetic resonance images of the abdominal aorta taken over several cardiac cycles to detect the perfusion of the arterial flow into the aneurysm sac. This procedure as a clinical screening is costly and is invasive with use of a catheter to inject the contrast medium [12]. Most of the time there is no problem with the EVAR: the stent is well seated and the endoleak condition does not exist. It is therefore desirable to have an effective screening method for endoleak that can be conducted on demand in an outpatient setting with minimal use of time, facility and personnel resources. This particular application has been titled the "Aortowatch" in the NSF sponsored project through the ASSIST Center [13].

A second potential application of a wireless ultrasonic mote is to monitor progress of incorporation of an engineered cardiac tissue graft into a damaged or infarcted region of native heart tissue. The article describes "the design and fabrication of a vascularized cardiac stem cell (CSC) patch combining stem cells with engineered biomimetic microvessels (BMV) [14] . The researchers further show that BMV–CSC patch can engraft on the epicardial surface of the

infarcted left ventricle and release stem cell factors to the scarred myocardium after myocardial infarction (MI), inducing cardiomyocyte proliferation and enhanced blood vessel formation in the peri-infarct region as well as at the host–patch interface compared with conventional CSC patch treatments." What is missing (the unmet need) for further advancement of this novel device for post-MI regeneration is the capability to monitor the regeneration of the cardiac tissue in vivo without damaging the tissue with a biopsy or sacrificing the animal. The regeneration of the tissue in the vicinity of the graft might be inferred in-vivo from improvement to cardiac signal flow detected using three-lead electrocardiogram measurements made periodically. A wireless implantable device that is powered by ultrasound and communicates by ultrasound could make these measurements every few milliseconds for two to three cardiac cycles before needing to replenish the energy storage. This particular application concept has been titled "Cardiopatch" for the NSF funded project. The Aortowatch and Cardiopatch devices share much of the same electronics, including a low power analog-to-digital converter. Only the analog front-end connections at the patient are slightly different: connecting to an electrode instead of an ultrasonic transducer. It is reasonable to assume that the same basic integrated circuit (IC) design can be used for both applications with minor modifications.

1.2 Challenge of a Wireless Implantable Device for Deep Tissue Applications

The key functional elements the wireless implantable device must incorporate are wireless power receiving and conversion, wireless data transfer (uplink) to an external unit, and a clinically significant measurement or therapy. In the case of measurement, the quantity of interest could be a distance across a vessel lumen, or it could be an electrostatic potential reflecting cardiac electrical signal dynamics. In the case of therapy, the action could be an electrical signal to stimulate a nerve or to stimulate heart tissue for synchronization.

The amount of energy needed by the device to accomplish its measurement or therapy purposes will dictate the size of the energy reservoir and the time between charging events. A practical implementation would provide a very low power state during the time between measurement events in order to conserve power. The ability to run from low voltage is also important. Reasonable voltages for pulse-echo ranging or data uplink are ± 3V. Depending upon the CMUT device, a DC bias voltage up to 40V may be required for device operation. There is work demonstrating voltage pre-bias of the CMUT [15] [16] [17] which is a key enabler of "bias-free startup" of this device. If pre-biasing is available, some additional DC voltage biasing (bootstrap) in the range of 10V - 20V could be provided by a charge pump after initial startup to adjust power conversion ratio to optimal values and allow for transducer variation due to manufacturing tolerances.

Another very important consideration is biocompatibility of the device. Silicon devices such as the CMUT and the IC are already passivated with oxides or nitrides of silicon, which are stable in the highly variable chemical environments found in biology. Interconnect and other passive components, however, will not be so well protected – they will need to be coated with a biocompatible - electrically insulating film such as parylene [18]. Use of this film is compatible with the acoustic performance because it is very thin relative to the acoustic wavelength. The additional loading from a thin film of biopassivating material, with similar viscoelastic properties to tissue also should not affect the performance of the device because tissue and fluid already loads the membrane.

The remaining challenge is to design a form factor that allows for transcutaneous delivery and attachment, whether by surgical implantation or endoluminally by catheter.

1.3 Contribution of this Work

The objective of this research is to provide proof-of-concept using ultrasound for the three primary functions of an implantable, wirelessly powered electronic microdevice for recording and transmitting clinically relevant data, using CMUT technology. In meeting this goal, it is acceptable to demonstrate each function in isolation from the others. The justification for running this kind of experiment before committing to an integrated circuit (IC) design implementation, is that IC development is expensive in time and resources. Exploring design tradeoffs using discrete commercial off-the-shelf (COTS) components and surface mount printed circuit boards saves time and research funding in the long run, at a minimal impact to schedule. The unmet need motivating this work is to demonstrate each functional element for this design individually in a simulated tissue environment (oil) using COTS components and the CMUT to provide a benchmark for the IC performance. This thesis reports the strategies and results for these proofs-of-concept demonstrations of ultrasonic power delivery, pulse-echo ranging with a real EVAR kit, and biphasic pulse communications.

1.4 Thesis Organization

This thesis describes laboratory proofs-of-concept for a wireless implantable device that uses ultrasound for three functions: power delivery, communication and measurement of a clinical parameter. The second chapter provides the background information to understand the motivations for use of ultrasound in this application and explain the selection of the capacitive micromachined ultrasonic transducer (CMUT). It also contains some information about the modeling of the CMUT in an electro-mechanical system, since this modeling capability is key to the design of the supporting electronics hardware. The third chapter presents the design approach used to receive acoustic power and convert it to electrical power for charging a

reservoir capacitor, and the reasons for the selection of this particular architecture. It describes the experimental setup for demonstrating power conversion using COTS components and some of the improvements made in power conversion ratio during the process of discovery. The fourth chapter describes the considerations for wireless communications uplink, and provides support for the biphasic pulse approach selected. Experimental setup diagrams are explained and results from the laboratory proofs-of-concept are discussed. The fifth chapter expands on the clinical applications of the deep implantable device, namely endoleak monitoring in EVAR stent-grafts. The sixth chapter provides a plan for the integrated circuit (IC) implementation, shows some key circuit schematics with explanations of their operation, and discusses why a particular industry process, the Taiwan Semiconductor Manufacturing Corporation (TSMC) BCD018 Gen 2, is the preferred process technology for implementing this IC. The seventh and final chapter provides concluding statements and points to future work needed to implement this technology. This future work includes design, fabrication and testing of the IC for the implantable, integration of the IC with a custom CMUT and other passives into a deliverable device, and design of the external unit for power delivery and communication.

CHAPTER 2. Background Information

This chapter presents some background information to understand the motivations for use of ultrasound in this application; and explain the selection of the capacitive micromachined ultrasonic transducer (CMUT). It also contains some information about the modeling of the CMUT in an electro-mechanical system, since this modeling capability is key to the design of the supporting electronics hardware. This background includes analysis of how much ultrasonic energy is available for charging the mote, and how that energy is expected to change as a function of frequency and depth in tissue due to attenuation. The limits placed on biological exposure to ultrasound will limit the energy transfer to the mote as a function of depth and ultrasound frequency. The axial and lateral resolution and focal spot size determined by ultrasound frequency have important implications for estimating resolution of pulse-echo distance measurement – that is, how much relative movement in the implant or tissue can we discern. These also have implications to the capability of an external device to focus ultrasonic energy on a small embedded mote.

The CMUT is selected in this work as the device for converting electrical energy to acoustic energy and vice-versa. The technology of this device is discussed, in particular what reasons motivated its use instead of the more established piezoelectric technology. The modeling of the CMUT in the electrical domain is discussed because this subject is key to designing electrical circuits interfacing to this transducer.

2.1 Key Ultrasound Concepts

Ultrasound is acoustic energy that propagates in a medium with a frequency higher than what is audible to humans, typically covering a range from 20kHz to ~1GHz. The frequencies of interest for biomedical imaging, i.e., imaging of tissues and organ systems, and also for the

implantable device application range from about 1MHz up to 10MHz. The reason for this practical limitation in frequency range for deep tissue imaging, or implantables, is the attenuation of ultrasound power increases more than tenfold over this limited range, from < 1 dB/cm at 1MHz to > 10 dB/cm at 10MHz [19]. More attenuation means less power reaching a deeply embedded device, so use of a lower frequency will increase range for a given transmit power. Higher frequency can also be a challenge for the power electronics accomplishing the conversion from acoustic to electrical domain, because the parasitic capacitors and logic delays become more significant with increased frequency. Higher frequencies do have an important role in communication and pulse echo ranging. For communication, the bit rate can be increased so that communication periods are short and power can be saved. Range measurements benefit because the spatial resolution improves with frequency.

Acoustic energy reflects from and is refracted at interfaces between two materials or different tissue types due to differences in their acoustic impedances. A good discussion of this subject can be found in Cobbold [20] . This behavior of "sound" is similar to how light is reflected or refracted at interfaces where the property η (index of refraction) changes. Acoustic impedance is calculated as "$Z_{AC} = \rho c$" where the term "ρ" is the density and "c" is the speed of sound in the medium. The speed of sound in tissue is relatively constant, so tissue density would seem to be the primary factor in the reflection and refraction that forms the basis for ultrasonic medical imaging. If there is only one element that serves as both transmitter and receiver, the analysis is simpler: the angle of reflection is the angle of incidence; so, provided the wavefront is normal at the reflector it will return to the transmitter, now turned receiver. At the interface between two acoustic materials, the ratio R_P of reflected pressure "P_r" to incident pressure "P_i" at a normal angle of incidence is:

$$R_P = \frac{P_r}{P_i} = \frac{Z_2 - Z_1}{Z_2 + Z_1}$$

Some easy cases that proved useful in this study are: 1) propagating from tissue to metal (such as stent) – the reflection is 100% and the return phase is identical to the transmit phase, and 2) propagating from tissue to air (which has a very low impedance), the reflection is 100% but the phase is inverted. The reflected energy in the first case provides the time signal used to measure distances to and characteristics of the blood-tissue-implant interfaces. It is expected that the metal stent providing support structure for a vascular implant device will be very echogenic. Blood is not very echogenic, but the blood tissue interface is. So, it is likely that an ultrasonic rangefinder will be able to discern both the implant and the opposing side of the artery at a range of 30mm. The second case of tissue-to-air was used in what is called "pitch-catch" experiments using two transducers, one operating as transmitter and the other as receiver, for ultrasonic communications. It is important to make note of the phase inversion as it becomes important for pulsed communications.

Next is the consideration of the spatial resolution of the range measurement application and power delivery, which is closely related to the wavelength. The wavelength of ultrasound energy "λ" as a function of frequency "f" and speed of propagation "c" is calculated as: $\lambda = c/f$. As noted previously, the speed of sound is found to be relatively constant in biological media (blood, tissue) over the frequency of interest, and can be approximated as 1.54 mm/μs. Therefore, the wavelength of 1MHz ultrasound in tissue is 1.54 mm. The wavelength of the ultrasound determines the ability to focus acoustic energy on a spot, like a small implantable device. The depth of field of the focal area is $DOF = \frac{8\lambda Z^2}{D^2}$, and the lateral width of the main lobe of the focused ultrasound is $W = \frac{2\lambda Z}{D}$. From these equations one can roughly approximate

the volume of reasonable power reception for the implantable device for energy focused inside the far field: at a range of 10 cm using a 4 cm wide 1 MHz linear probe, the size of the ellipsoidal shaped focal volume should be about 8 mm laterally and 8 cm axially. This is a broad area of illumination inside of which the implantable device can be powered, but the result shows the capability to focus in the lateral and elevational planes is most important.

The wavelength of the ultrasound also determines the resolution for measuring distance to features from reflected energy. The acoustic pulse from a single, small 3 mm^2 transducer will radiate out in almost spherical wavefronts when the range is beyond the near-field to far-field transition. This transition to far-field occurs at approximately $Z = \frac{D^2}{4\lambda}$ For D = 1.8 mm and frequency of 3 MHz, this transition occurs about 2 mm from the CMUT. The location of this transition is important because one can assume beyond it, the acoustic pressure incident on the reflecting surface will be inversely proportional to range, and the reflected pressure received by the CMUT will be further reduced, also proportional to range. Even without attenuation, the pressure of the return signal would be expected to vary by the ratio of the furthest object over the nearest object. If the opposite surface of the aneurysm sac (artery) is at a range 35 mm, and the nearest surface of the EVAR is at 7 mm, then the return signal pressure varies five-fold due to propagation alone. Add attenuation due to scattering of signal from the echogenic structures of the EVAR and the return signal could vary at least an order of magnitude. A time-gain compensation in the receiver amplifier will be needed to accommodate this signal variation.

The axial (distance) resolution is determined by half the pulse length of the emitted pattern for pulse-echo ranging. Therefore, a 3 MHz biphasic single-pulse with a pulse length of 0.5 mm should provide a distance resolution approaching 0.25 mm. Arteries are compliant, that is they expand and contract to accommodate pressure and volume changes from cardiac output.

In a 25 mm vessel such as the aorta, a few mm of change in arterial diameter would be within expectation over the systolic-diastolic cycle. The resolution of ultrasound is more than sufficient to detect this expansion and contraction in arteries or grafts during the cardiac cycle. That measurement is the main objective of this implantable device.

The return time for a reflected ultrasound pulse from the nearest feature to be imaged sets the time needed to change between transmit mode and receive mode for the electronics. For example, to register an echogenic feature 7.5 mm from the transducer face will require the electronics to make the mode change in less than 10 μs. The range of 35 mm to the opposite side of the artery implies a return time of 45 μs. A record length of 51 μs, sampled every 100 ns would generate about 512 or 2^9 samples with 8 bits resolution. We will have to revisit whether the device needs to uplink 4096 bits for every range measurement – as it will have implications for power reservoir size.

The risk of biological effects from diagnostic ultrasound are inconsequential based on a long history of use. The FDA stipulates limits with the aim of continuing to minimize these effects. The limits impact the ability to deliver energy to an implant. Spatial-peak temporal-average, I_{SPTA}, is defined as the highest intensity measured at any point in the ultrasound beam averaged over the pulse repetition period. This limit is closely related to the magnitude of thermal bioeffects and it applies primarily to the continuous wave pattern that will energize the implant. The I_{SPTA} limit for diagnostic purposes is 7.2 mW/mm^2. When we consider a 3 mm^2 transducer, the available energy is more than 20 mW at the limit. This level is more than sufficient to energize the power conversion electronics and have surplus to charge a battery. When we compute the pressure amplitude at the I_{SPTA} limit in tissue using an acoustic impedance Z_{AC} = 1.5 MRayl, the maximum amplitude is: $P_{AC} = \sqrt{2 * Z_{AC} * PWR}$ = 150 kPa. The

experiments with ultrasonic power delivery described in this work used a commercially obtained focused transducer and achieved acceptable power at incident levels less than the I_{SPTA} limit. This fact was determined by pressure measurements using a calibrated hydrophone, and these measurements did not exceed 140kPa amplitude. The other biological safety limit, mechanical index (MI) helps to reduce likelihood of a nonthermal bioeffect, such as cavitation. It is defined as the maximum value of the peak negative pressure (in MPa) divided by the square root of the acoustic center frequency (in MHz), with a diagnostic limit of 1.90. It is primarily encountered with single pulses of high amplitude. Based on lab measurements with the hydrophone, the pressure output of a single CMUT element driven with a ± 4V pulse does not exceed a 100 kPa within a few millimeters of the transducer, so there is ample margin to the MI limit in these experiements.

2.2 Capacitive Micromachined Ultrasonic Transducer

The ultrasonic transducer is a key element, along with the electronics, in the implementation of the ultrasonic mote. Two competing technologies exist for ultrasonic transducers. The established and more widely available piezoelectric technology is based on the property that certain materials change their dimensions in response to application of an electric field. The newer CMUT technology is based on the electrostatic actuator, which is simply a capacitor with one fixed and one movable plate. As a discrete device, it is only available in research laboratories at this time. Four advantages of a CMUT in this biomedical implant application are: 1) the biocompatibility of the materials used in its construction; 2) its wideband frequency response; 3) the thin form factor and potential for bonding it directly to the electronics

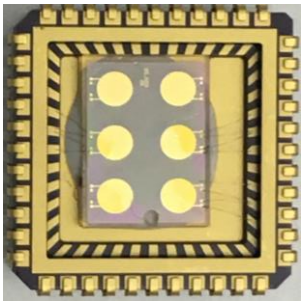

Figure 3. CMUT used for experiments.

to further reduce device footprint; and 4) cost and reliability of the manufacturing technology. The biocompatibility is inherent in the use of mechanically and electrochemically stable silicon oxide and silicon nitrides, and in metallization consisting of alloys of titanium and nickel which are also used for biomedical stents [21]. An antifouling surface for the acoustic membrane (such as PEG) is probably not needed since bio-fouling should not affect the acoustic loading. The second advantage, wideband frequency response, is due to the principle of operation with a thin membrane loaded with a viscous fluid. The benefits of wideband response are to device communication with the outside world and function of the device transmitting and receiving short pulses for distance measurements. The third advantage of low profile and vertical stacking of the CMUT upon the electronics has obvious advantages in a space constrained application. The fourth advantage of high yield and reliability at a low unit cost comes from use of silicon manufacturing technology.

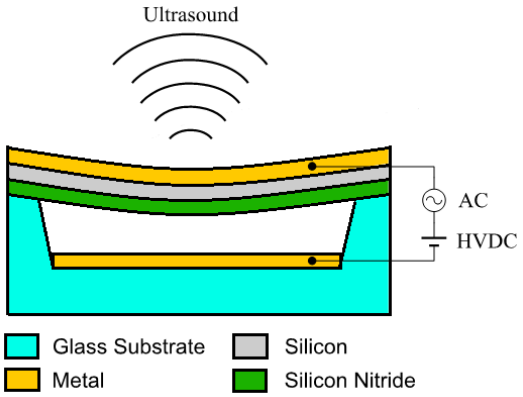

Figure 4. Cross section of CMUT showing key layers

The CMUT is an electrostatic actuator with a vacuum gap. Each element consists of a group of interconnected cells. The CMUT element we used in these studies consists of 533 (or 262, for the smaller) parallel cells spaced at a pitch of 70μm. The movable diaphragm of each cell has been made of various materials: metal, nitride, crystalline and poly crystalline silicon to name a few, but there is always a thin layer of insulating material like silicon nitride lining the gap to prevent an electrical short. The diaphragm is suspended above the gap by posts placed between the cells. The dimension of the gap (~180 nm) relative to the diameter of the freely moving diaphragm (~60 μm) is between two and three orders of magnitude smaller. The thickness of the silicon diaphragm (~1.5 μm) is an order of magnitude larger than the gap. The deflection of the plate is very small relative to the freely moving area of the diaphragm between the anchoring posts, and this allows some important simplifications in the analysis of the mechanical behavior.

The mechanical behavior can be described mathematically by the second order differential equations of motion for a damped spring, representing the acousto-mechanical behavior of the membrane vibrating in one dimension. The mechanical behavior is coupled with

$$(m_{\mathrm{ps}} + m_{\mathrm{fl}})\ddot{w} + (b_{\mathrm{ps}} + b_{\mathrm{fl}})\dot{w} + k_{\mathrm{ps}}w = \frac{1}{2}\varepsilon_0 A_{\mathrm{el}}\frac{U^2}{(h_{\mathrm{gap}} - w)^2} + F_{\mathrm{ext}}.$$

the electrostatic force that depends upon the distance between the plates. The equation follows the analysis of Lohfink and Eccardt [22], where ω is the average displacement of the membrane; The different mass terms, m_{ps} and m_{fl}, represent the respective masses of the membrane and the

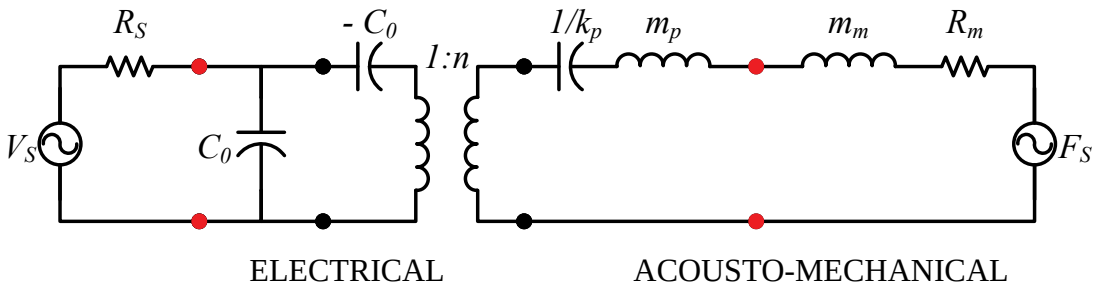

Figure 5. Electrical model of acoustic transducer replacing mechanical terms with electrical elements.

fluid loading the membrane. The b_{ps} and b_{fl} terms represent the acoustic impedance or damping terms of the membrane and the fluid. The k_{ps} term represents the net spring constant of the membrane, following Hooke's Law, which relates the displacement of the membrane (from its relaxed state, h_{gap}) to the sum of normal forces on the membrane from electrostatic and acoustic sources (F_{ext}). We take the displacement to be the average displacement over the membrane, and this is known as the "piston" model. The perimeter of each cell is fixed and maximum displacement is at the center, for the primary mode of vibration. The second order equation for membrane displacement has a counterpart in the electrical domain, where the charge "Q" is the variable. In that second order equation, inductors, resistors and capacitors occupy the same positions as mass, viscous damping and spring constant, respectively. To facilitate simulation and design, the mechanical and electrical portions of the circuit can be converted to all electrical components, using a transformer to represent the coupling factor between the two domains. The figure below is a schematic of the devices in the simplified linearized model of the CMUT, adapted from [23].

It is important to appreciate the effect of fluid loading on the frequency behavior of the CMUT. For the gas sensor devices used in this research, the frequency response measured in air was a sharp, high Q-factor peak at 5 MHz. Air is a fluid, but it has minimal damping effects, so it might as well be vacuum. When these devices are immersed in oil, the sharp peak disappears, replaced by a broad peak at ~2 MHz. This peak value is less than half the resonance frequency, and the fractional bandwidth is much greater at 93%, implying very low Q. The shift to a substantially lower frequency and spreading of frequency response happens because the fluid adds appreciable mass to the membrane, and the viscous non-elastic qualities of fluid cause energy absorption. The lower Q may be a showstopper for a gas sensor application which detects levels of volatile compounds by a shift in the resonant frequency. But low Q is desirable for this application and for imaging and communications applications in general because of the wide bandwidth. For example, even though the peak of the CMUT frequency response was 2 MHz, it is acceptable to use a piezoelectric transducer tuned to 1.3 MHz to deliver power to the CMUT. The lower frequency fits nicely with the goal of delivering power to a larger spot-size deep in tissue with minimal losses due to absorption. The same CMUT can also be used to transmit biphasic pulses at 3MHz, which is on the high end of its response curve. For

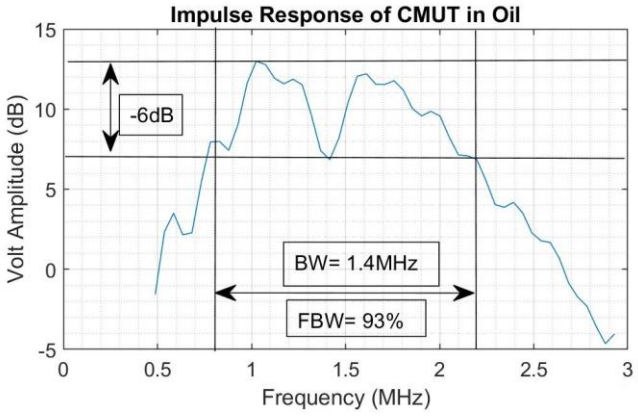

Figure 6. Wideband response (0.75 MHz to 2.2 MHz) of CMUT in oil

applications requiring a higher center frequency, the CMUT has additional bandwidth capability from collapse mode if bias voltage is further increased. In collapse mode, the resonant frequency increases more than 2x because the center of the membrane touches the bottom electrode and becomes fixed, so that the vibration mode changes to a higher frequency. The figure shows the frequency response in air at two bias voltages. Note the appearance in the 56 V data of a broad peak at 12 MHz. This same frequency translation occurs with the fluid loaded membrane as the peak frequency response moves from 2 MHz to 5 MHz. The collapse mode is very useful in this work for proving the full biphasic communications concept using the commercially available LTC6820 protocol device, which needs higher frequency and bandwidth than conventional mode could provide. Collapse mode may not be optimal for wireless power because ultrasound attenuation increases with frequency and transition losses in the power converter will increase.

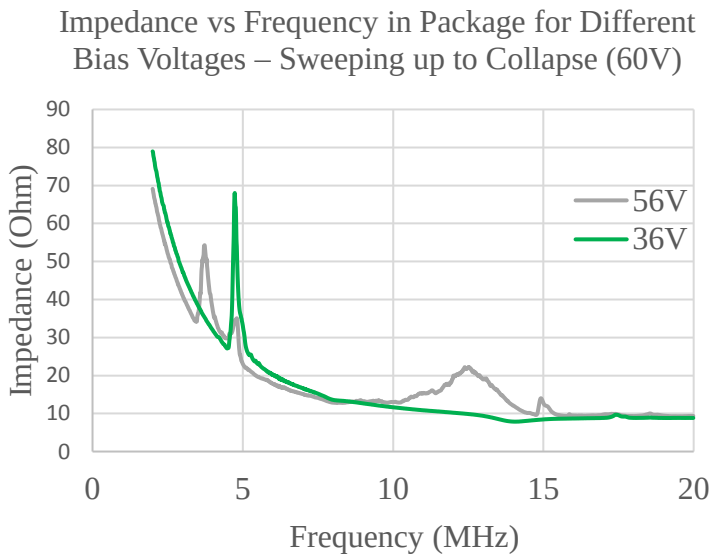

Figure 7. Frequency response in air for normal and collapse modes showing high frequency capability of collapse mode.

The CMUT devices have a fundamental need for a voltage bias in order to operate as a power receiver. Without further development of the device, the need for this voltage supply could be in conflict with the idea of a remote device as being self-biased ready to generate

electric power upon receipt of ultrasonic energy. In this proof-of-concept, we used an external power supply that varied from 30 V to 50 V to give conventional mode operation for the CMUT. Future work can address this unmet need through the use of pre-charged CMUTs. The conclusions contain a brief discussion of possible approaches for pre-charged CMUTs found in the literature.

There are a number of ways to manufacture the CMUT using the MEMS toolkit of surface and bulk micromachining. One of the simplest techniques is a low temperature, low step count process employed by the IMIST group at NC State [24]. It uses a combination of bulk and surface micromachining techniques. At the core of this fabrication process is anodic bonding of a borosilicate glass wafer with a silicon on insulator (SOI) wafer. Anodic bonding uses elevated temperature and voltage to cause mobile ions in the borosilicate glass to migrate into the SOI wafer, first electrostatically bonding the two wafers, then chemically bonding them. The main advantages of anodic bonding technology is that it employs lower temperatures that will not destroy metallization, and it is somewhat less sensitive to the smoothness of the two wafer surfaces when compared with fusion bonding. Prior to bonding, cavities and interconnect channels are etched into borosilicate wafer, followed by patterning of the bottom electrode in a metal deposition lift-off process. The resulting CMUT vacuum gap is determined by the depth of the cavity in the glass minus the height or profile of the metal interconnect. The walls of the cavities become insulating support posts after the next step. The completed bottom plate is then anodically bonded to the device side of the SOI wafer, with a thin nitride layer deposited on the silicon as a dielectric insulator and to prevent contamination of the membrane with impurities that could outgas over time. The thin monocrystalline silicon device layer (~2 μm) on the silicon oxide determines the thickness of the membrane. After bonding, the SOI wafer, also called the

handle, is mechanically polished then chemically etched back to expose the previously buried oxide now covering the thin membrane. During the bonding, gases are released that become trapped in the cavities and lead to their pressurization. These gases are purged by opening a vent to the cavities in the next step, which also exposes the buried electrode and allows contact to it. The following steps etch the (buried) oxide on the handle wafer and make electrical contact to the membrane or top plate, finally adding a thin silicon nitride passivation layer after pulling a vacuum on the cavity, to seal it off from atmospheric pressure and to electrically isolate the top and bottom electrode metals. With a small increase in cost and complexity, the borosilicate glass wafer can have predefined thru-vias allowing the CMUT to be bonded directly to its electronics using "flip-chip" technology and saving area in small form factor applications [25]. The possibility of heterogeneous integration is one of the key advantages of using the CMUT instead of piezoelectric technology, besides the superior device performance. The biological disadvantage from the rigidity of both piezoelectric and CMUT technology is partially offset by the compactness of the CMUT technology when it is integrated with the supporting electronics. In either implementation, off-chip passives can be connected to the electronics through schemes metallizing (Platinum) a biocompatible flexible substrate (PDMS), followed by passivation of the entire assembly with a bioinert conformal composite such as Parylene-C with Alumina [18].

CHAPTER 3. Ultrasonic Wireless Power

3.1 Power Converter Architecture

A key requirement of the implantable device is wireless power delivery. The stored energy need only last as long as it takes to make the clinical measurements and transmit the data. Multiple cycles of power delivery followed by a reasonably long measurement phase are possible. A wireless ultrasonic power recovery scheme is demonstrated in oil using a single element CMUT and a circuit made with commercially available devices: diodes, transistors, an inductor and a comparator with open drain output for the boost regulator. The 2-mm diameter CMUT element with area = 3mm^2, a diode rectifier bridge and an inductor-based boost circuit form the power conversion circuit. In these experiments, the bias voltage for the CMUT is supplied externally, but the plan is to develop a pre-charged device to eliminate the bias.

The inductor-based buck-boost circuit is selected over the capacitor-based charge-pump voltage step-up because it does not require any mode changes (i.e., doubler, tripler, fractional) to provide power over the wide range of output voltages encountered in charging a battery. This buck-boost circuit typically operates in discontinuous conduction mode, which means the inductor current starts from zero at the beginning of each cycle.

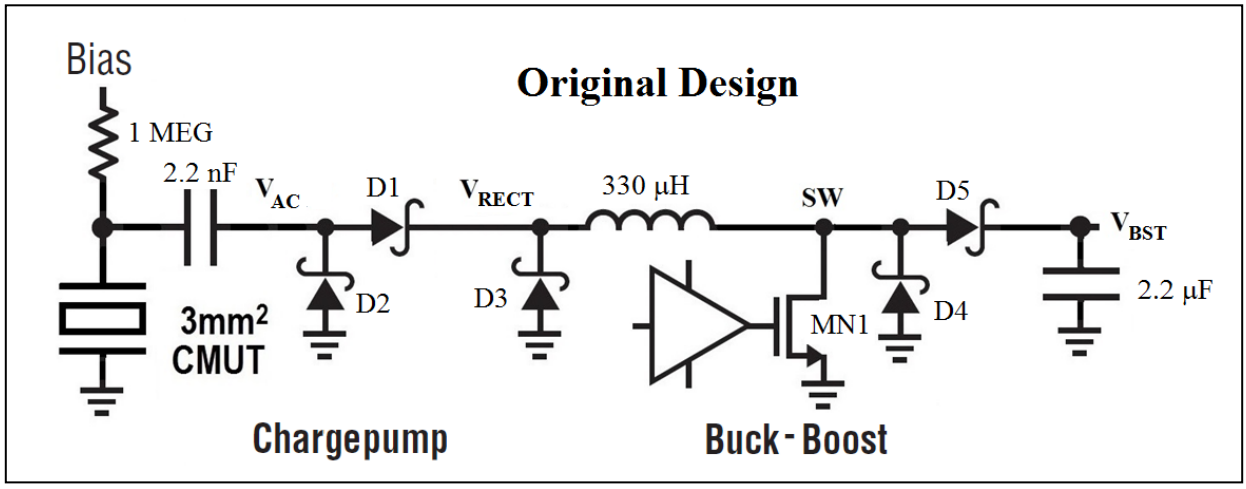

Figure 8. Power converter circuit schematic diagram. Original circuit used only diodes for rectification.

The operation, which is hysteretic based on the input voltage, can be briefly described as follows. During the positive phase of the voltage at V_{AC}, the switch MN1 turns on and the inductor current increases, supplied to V_{RECT} from the CMUT through the 2.2nF coupling capacitor and diode D1. During the negative phase of V_{AC}, the switch turns off and the inductor discharges current to the output V_{BST} through D5. The inductor current is supplied by D3 during the negative phase of V_{AC}. Also, during this phase of V_{AC}, the charge on the CMUT and 2.2nF coupling capacitor is replenished through diode D2. In this manner, the acoustic energy is converted to current and this electrical energy is transferred to the output using an inductive storage element.

3.2 Experimental Setup

On the power recovery circuit, we investigated two different sizes of CMUT elements, variations in transducer excitation frequency, CMUT bias voltage, circuit component selection, and active vs. passive rectifier design. During our experiments, the current supply for the boost circuit (LMV7235, Texas Instruments, Dallas, TX, USA) was provided separately, but it could be supplied from the boosted output or from a rectified input. The ultrasonic signal was

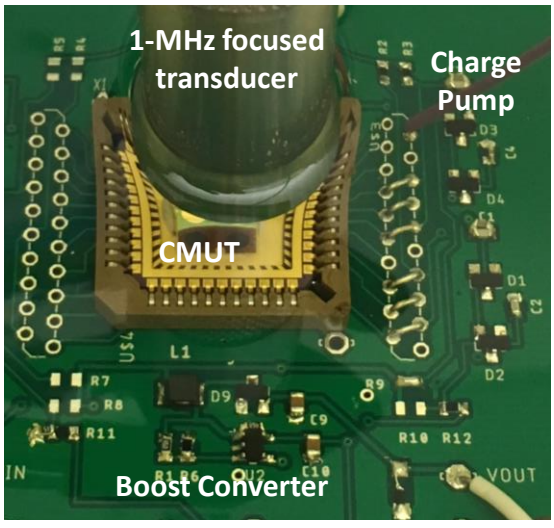

Figure 9. Photo of experimental setup for acoustic converter circuit and transducer. Immersed in oil.

provided by a 1MHz, 25mm focus, 12mm diameter, commercial piezoelectric transducer (A303S, Olympus, Waltham, MA, USA) driven by a waveform generator (33500B, Keysight, Santa Rosa, CA, USA) set to 10 V peak-to-peak and 50 Ohm load. The pressure field from this transducer was measured in oil using a hydrophone + preamplifier (HGL-0200 & AH-2010, Onda, Sunnyvale, CA, USA) to verify that the power did not exceed the 7.2 mW/mm^2 ISPTA limit. The pressure was found to be relatively uniform over the 1.5 mm diameter of the CMUT at

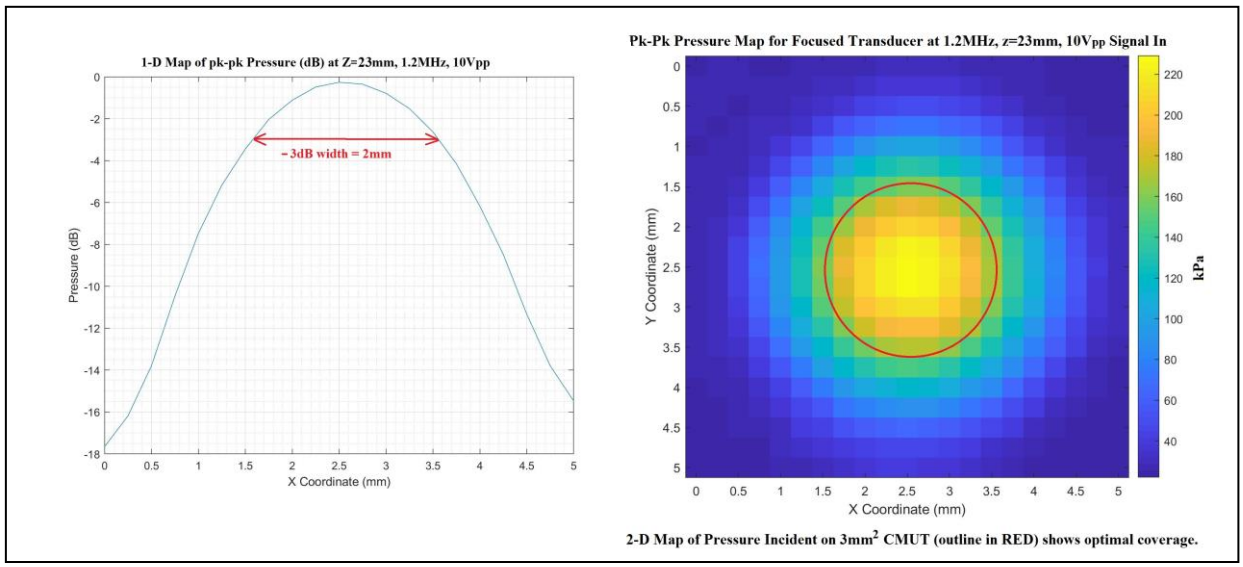

Figure 10. Cross section graph and colormap of pressure seen by CMUT laterally at an axial distance of 23mm

the 23 mm range where the experiments were run. The peak-peak pressure and peak power at the driving voltage of 10 Vp-p were measured to be 276 kPa and 6.2 mW/mm^2 at a distance of 17mm from the transducer face. The main lobe width of the lateral/azimuthal pressure distribution at 1.3MHz was consistent with the transducer geometry. Full-width half max is computed as $2\lambda z/D = 2*1mm*23mm/12mm = 4mm$. The length of the focal area was also consistent with theoretical depth of field. DOF= $8F^2\lambda = 8*2^2*1mm$. What these two results imply is the sensitivity of power recovery to mote placement (or external transmit focus) will be much higher in the lateral dimensions than the axial (depth) dimension.

3.3 Key Results

The highest power achieved (1.1 mW) used the active rectifier at bias voltages approaching CMUT collapse, and at excitation frequencies (1.2 MHz) where we find the center frequencies of the transmitter and the CMUT match. These results were achieved using a 330 µH inductor and "active" rectifier Q1 on the chargepump input. The initial experiments used a Schottky diode at D1 between the V_{AC} and V_{RECT} nodes, but replacing this diode with a PNP transistor improved power conversion by a factor of three, from 300 µW to 900 µW. An additional 25% improvement to 1.1 mW was achieved by replacing the initial 470µH inductor with a 330 µH value. A key takeaway for the future design is that minimizing voltage drops

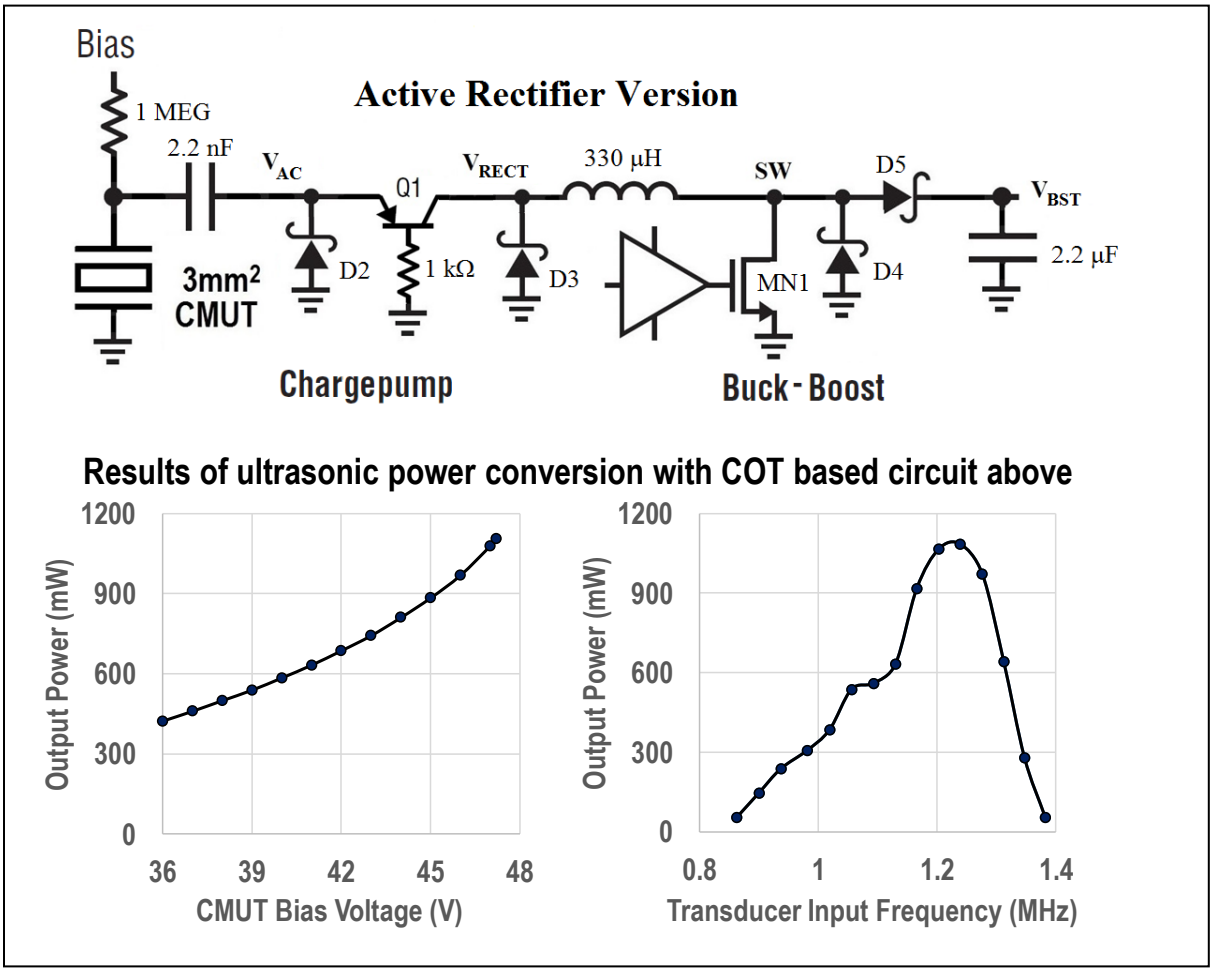

Figure 11. New power recovery circuit schematic uses an active rectifier. Results show a 4x improvement.

across the rectifying elements can yield large gains in power conversion. The integrated circuit can implement active rectifiers replacing each of the diodes in this circuit as will be discussed in chapter 6.

CHAPTER 4. Ultrasonic Wireless Communications

One challenge for implementing microscale implantable ultrasonic telemetry is getting data into and out of the remote device. To achieve robust data transmission, one needs to have unambiguous interpretation of when data is being transmitted – that is the start and stop of the data frame; and the bits, 1's and 0's should be transmitted in such a way that the data can be sampled unambiguously in the presence of amplitude distortion and variable latency. There are various methods for ultrasound that are compatible with continuous wave transmission, such as frequency shift keying (switching frequency between 1's and 0's) and phase shift keying, which is similar except with phase, and on/off shift keying [26]. To synchronize up, to determine which data represents the start of the frame and how to interpret a long chain of 1's or 0's, there are various digitally intensive techniques such as bit stuffing to ensure that the clock signal is recoverable from the data stream. The technique investigated in this work eliminates the need for all this complexity. It uses single ultrasonic pulses and inverts the phase to signal the data polarity. To distinguish between control signals like start and stop of transmission, and the data, two easily distinguished frequencies are employed. It also solves the problem of continuous wave transmission which would quickly drain the device's energy reservoir.

4.1 Wireless Uplink Considerations

Compared to the on-off shift keying techniques, the anticipated advantages of using this single-pulse system with phase indicating polarity is 1) increased data rate, as high as 500 kHz with data signal frequency of 3 MHz, and control signal frequency of 1 MHz, assuming the two types of pulses can be spaced at 2 μs; 2) better immunity to multipath interference, which could be a complication where highly echogenic structures such as bone are near the implant; and 3)

power efficiency because the communications can be concluded using a smaller number of pulses, less time and thus less energy.

4.2 Approach

A key aspect of the implantable device is the transmission of data collected during pulse-echo ranging to the external unit for diagnostic analysis and periodic monitoring. It is desirable for translation into the clinical setting to use a common bus standard, such as serial peripheral interface (SPI) and convert this standard to a "one-wire" differential protocol to drive the CMUT and generate pressure waves. The pressure waves will then be received by a second CMUT, converted to electrical signals and decoded to convert them back to the SPI signals.

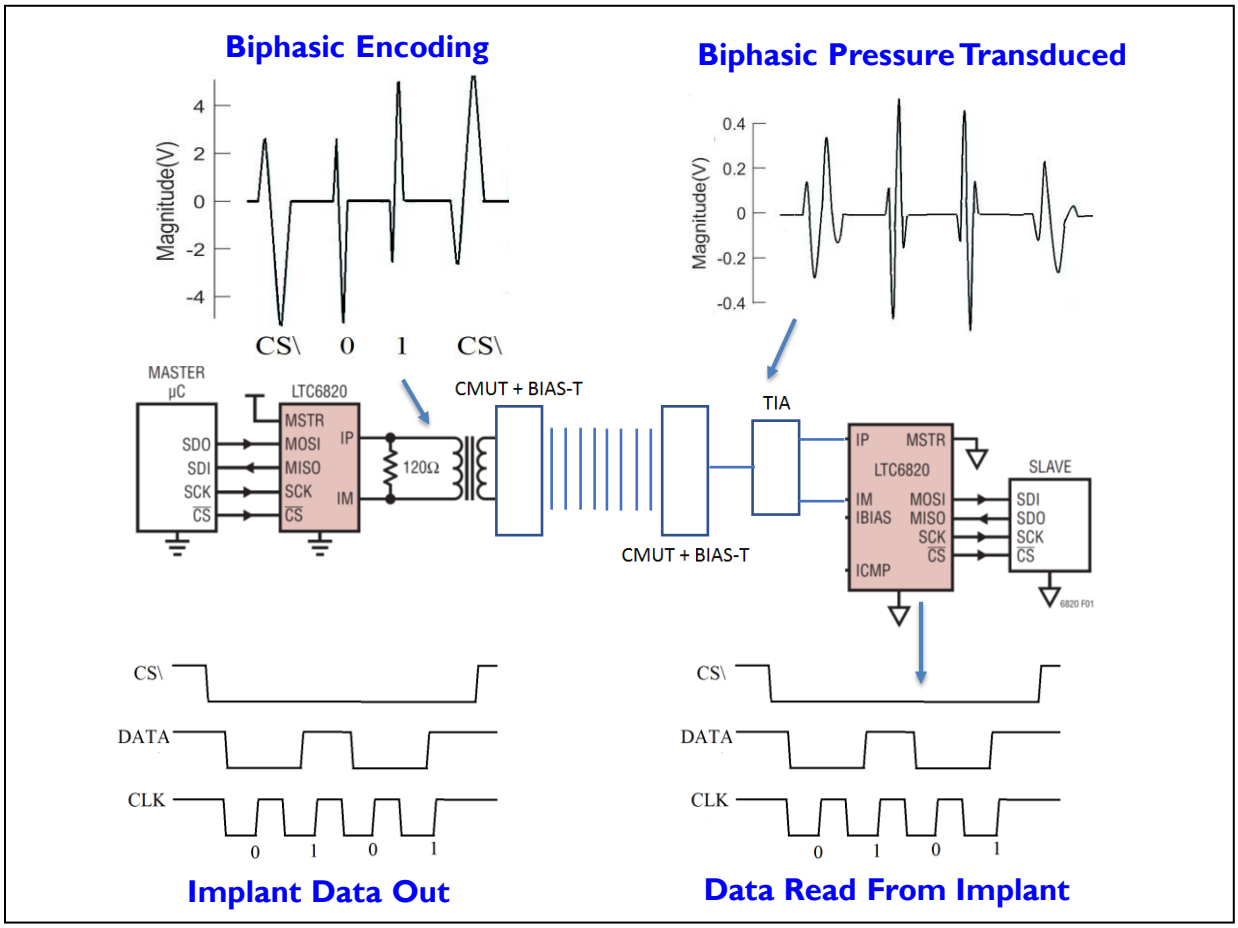

Figure 12. Signal flow diagram shows triangular shaped biphasic pulses to transmit side, and sinusoidal biphasic pulses at receiver.

The broadband characteristics of the CMUT are key to the use of an industry standard "IsoSPI™" protocol we selected, which is implemented in the protocol device (LTC6820, Analog Devices, Norwood, MA, USA) [27]. This "cable driver" communication concept uses single biphasic pulses with phase indicating polarity; and two distinct frequencies, 10 MHz and 3 MHz are used to communicate data and frame information, respectively.

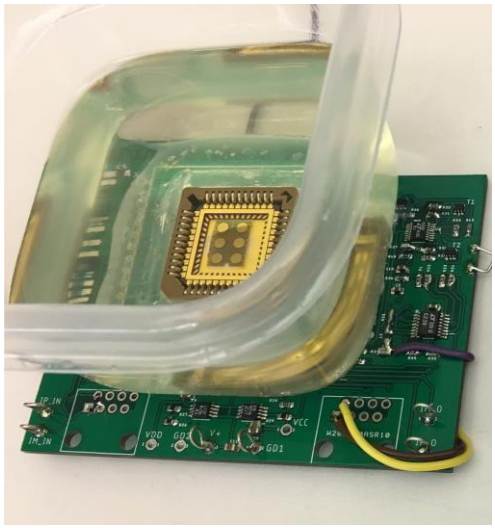

Figure 13. Experimental setup for biphasic pulsed communications, immersed in oil. Two CMUTs used, one each for transmit and receive. The acoustic signal is reflected from the oil-air interface.

4.3 Experimental Results

The wireless communications concept is demonstrated in an oil tank with two CMUTs, one for transmit and the other for receive. The frequency response of the CMUT (conventional operation) was compatible only with the chip-select feature of the protocol chip. The circuit demonstrated correct decoding of the biphasic pulse as shown in Figure 14. The experiments revealed that for a correct decode on the receiver side, the waveform driving the transmitting CMUT could not be a simple biphasic square pulse as generated by the commercial transceiver. This realization is important to the future IC design. In these experiments, to get a sinusoidal pulse at the appropriate frequency and shape on the receive CMUT, a sinusoidal pulse of a particular phase and a pure frequency was used on the transmit CMUT. Correct encoding on the

transmit side, which will eventually be done by the integrated circuit, will require a pulse shaping circuit that converts the square pulses into a triangular shape. In frequency domain, what this pulse shaper will do is convert the input waveform from a sinc(x) to a $sinc^2(x)$ to match the more limited bandwidth of the ultrasonic device. This need is not surprising, the CMUT is much narrower bandwidth compared with the pulse transformers used in the cable driver configuration for which the commercial protocol chip was designed.

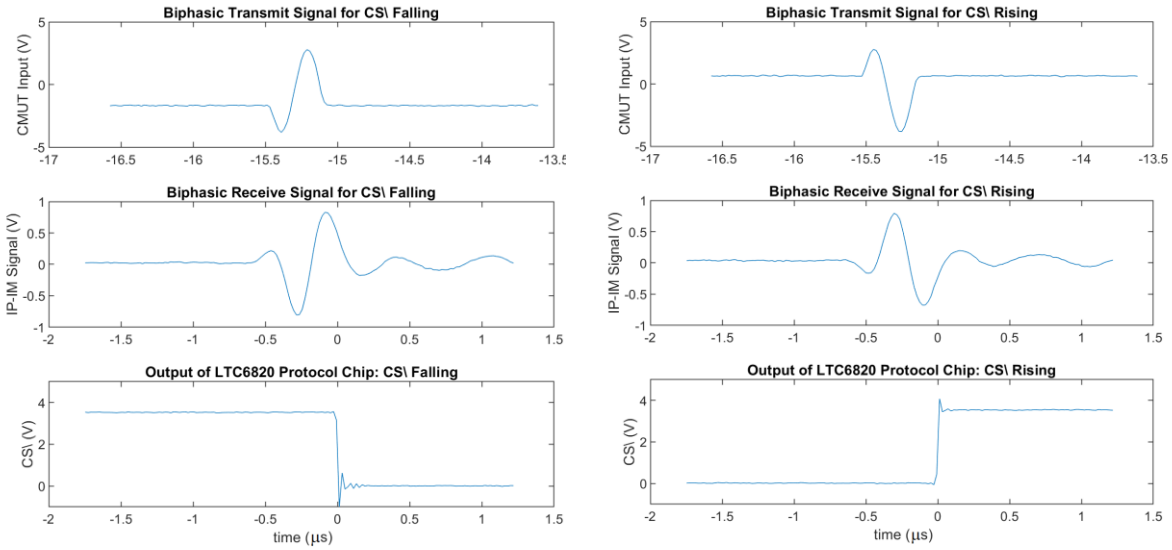

Figure 14. Oscilloscope recordings of transmit and receive signals in acoustic biphasic pulse communication. The protocol chip (LTC6820) response is the bottom trace.

The frequency range of the CMUT used this experiment and operating in conventional mode does not extend to 6 MHz, which is the minimum needed by the commercial transceiver for data communications. Therefore, the demonstration of decoding by the commercial transceiver was limited to the control signals at 2.5 MHz, which is within the bandwidth of the CMUT. It is, however, possible to test both data and control signal communications in a future demonstration using collapse mode of the CMUT. Collapse mode operation approximately doubles CMUT bandwidth, and translates the center frequency of the bandwidth to more than

twice that of non-collapse mode. The adjustments to the receive conditioning hardware are easy to make, but pressing priorities of designing the IC did not allow time for this experiment.

CHAPTER 5. Clinical Applications of Wireless Implantable Device

5.1 Monitoring for Endoleak in an EVAR Stent-Graft

A miniscule ultrasonically powered device integrated into the EVAR stent-graft, or delivered transcutaneously into the aneurysm sac prior to EVAR deployment, could provide on demand diagnostic information about the presence of endoleak. The diagnosis of endoleak would be based on static and dynamic measurements of the aneurysm sack dimensions and of the stent-graft inside the vessel lumen. Medical implantable devices can be incorporated into the EVAR stent-graft as described in US Patent 6,840,956 and polled with an external unit to record clinically useful data from ultrasonic measurements as described in US Patent 7,198,603. The approach described in these patents, however, is one of static measurement of pressure in the aneurysm sac, or blood oxidation level, or some other static parameter. This contribution of this work is different in that it proposes a series of lumen diameter measurements during a cardiac interval that can be used to infer the elastic response of the implant and/or the aneurysm sac to pulse pressure variation. In the presence of endoleak blood pressure will be equalized on both sides of the stent/graft and this condition should reduce the variation in distance over the cardiac interval compared with the “no endoleak” case.

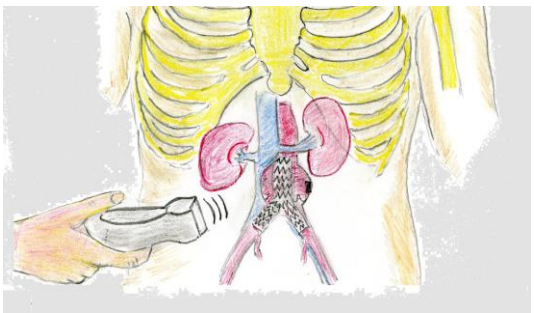

Figure 15. Proposed routine monitoring for EVAR endoleak requires an external handheld unit to transmit power and receive data. The implanted device (black rectangle) measures static and dynamic dimensions inside the aneurysm sac.

The primary goal of this experimental setup was to investigate the echogenicity of the EVAR device and the likelihood of measuring a differential distance across it and potentially across the aneurysm sac. The EVAR, immersed in oil to simulate blood, is exposed to single biphasic ultrasound pulses of ~3 MHz emitted by a single larger CMUT element excited with (±3V) at a range of 10 mm to 50 mm – the typical EVAR is between 20mm and 30mm in diameter. The setup for this experiment was similar to the pitch-catch used for the data communication, with one CMUT element serving in a transmit mode, and a second adjacent element served as receiver for returning ultrasonic energy. Ultimately, the integrated circuit will allow the use of a single CMUT by automatically changing mode from transmit to receive after the biphasic pulse is generated. The received signal is passed through a single stage of transimpedance amplifier to generate the voltage waveform portrayed in the figure.

The pulse-echo response to the EVAR stent-graft is shown in the figure. One notes that the signal returned from the trailing side of the EVAR is appreciably smaller amplitude ($1/4^{th}$) compared with the signal from the leading edge. This is due partly to 1/R spreading of the ultrasound since we are in the far field, but also to scattering of the signal returning from the far

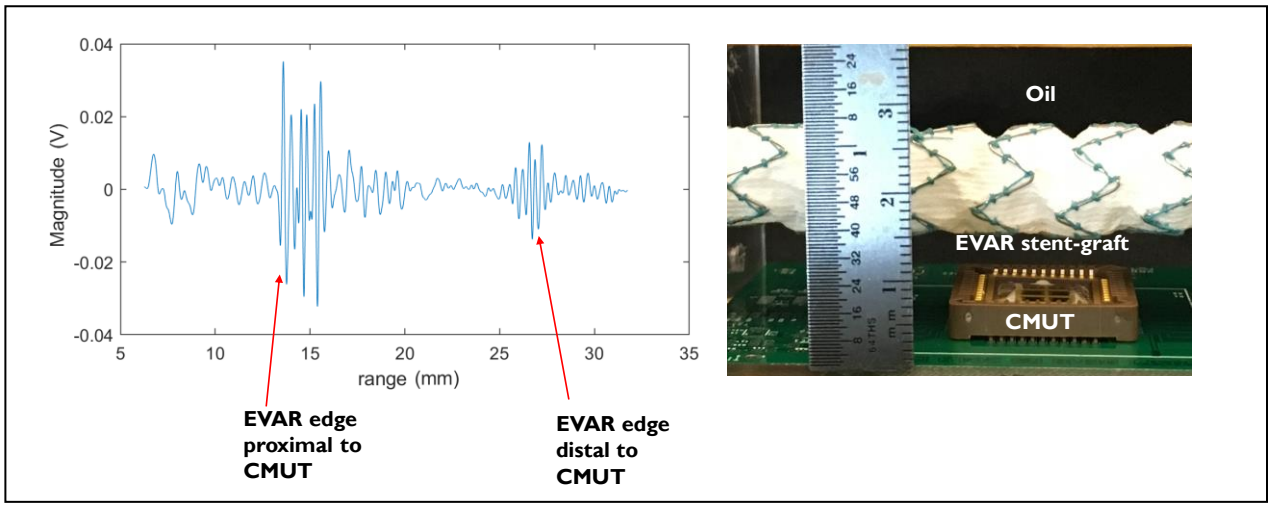

Figure 16. Waveforms showing pulse-echo signal returned from EVAR. Experimental setup (immersed in oil) is shown on the right panel.

side of the graft when it encounters the proximal side. This "attenuation" can be handled with suitable electronics in the IC – namely, a time gain amplifier. The metal stent structure is found to be highly echogenic. Investigations into the best way to represent these data for encoding and transmission are moving forward. Considering size, power and software/hardware flexibility, it is desirable for an external ultrasonic unit to make the data analysis while the implanted ultrasonic device merely measures and reports the clinical data.

5.2 Other Applications

A second possible application of a wireless ultrasonic mote is to monitor progress of incorporation of an engineered cardiac tissue graft into a damaged or infarcted region of native heart tissue. The device investigated by the Daniele group at NC State [14] for regeneration of infarcted cardiac tissue is "a vascularized cardiac stem cell (CSC) patch combining stem cells with engineered biomimetic microvessels (BMV)". The unmet need for further advancement of this novel device for post-MI regeneration is the capability to monitor the regeneration of the cardiac tissue in vivo without damaging the tissue with a biopsy or sacrificing the animal. It is proposed that regeneration of the tissue in the vicinity of the graft might be inferred in-vivo from improvement to cardiac signal flow detected using three-lead electrocardiogram measurements made periodically. Other measurements, such as impedance of the cardiac tissue – specifically looking at the development of intercalated disks in the patch, could also be indicators of tissue regeneration. A wireless implantable device that is powered by ultrasound and communicates by ultrasound could make these measurements every few milliseconds for two to three cardiac cycles before needing to replenish the energy storage. The Aortowatch device (project title for implantable device monitoring development of endoleak in the EVAR) shares much of the same electronics as what would be required here, including a low power analog-to-digital converter.

Only the analog front-end connections are slightly different: connecting to an electrode instead of an ultrasonic transducer. The flexible electrodes would be part of the patch itself; so, some mechanism to connect to these would have to be devised. But it is reasonable to assume that the same basic IC design can be used for this different application with minor modifications. These modifications would also include the length of data to be transmitted, perhaps only 2 bytes of 10-bit data are needed. Also, it may be necessary to increase the frequency of measurement to several hundred Hz to track the fast QRS and the ST segments of the cardiac electrical signal.

CHAPTER 6. Design and Fabrication of Integrated Circuit Implementation

6.1 Overall Design Objectives

The Wireless Ultrasonic Energy Converter, Data Logger and Transponder is intended for micro scale implantable biomedical applications which need on-demand data logging. One application is monitoring of endoluminal vascular aortic repair (EVAR) devices for development of leak into the aneurysm sac. This device interfaces with a CMUT to convert ultrasonic energy from an external unit to electrical power to charge a large value capacitor. When charging is complete, the device uses this stored energy to drive the CMUT in transmit receive mode to make dimensional measurements of the EVAR lumen and possibly the aneurysm sac to determine the performance of the EVAR. It then encodes this data and transmits it to the external unit after each measurement. To capture the dynamic element of sac dimensions in response to the cardiac cycle, the device needs to capture up to 30 measurements per second with each measurement taking less than 1 ms including the data uplink. For the long interval (30 ms) in between measurements, it switches to micro-power mode to conserve power.

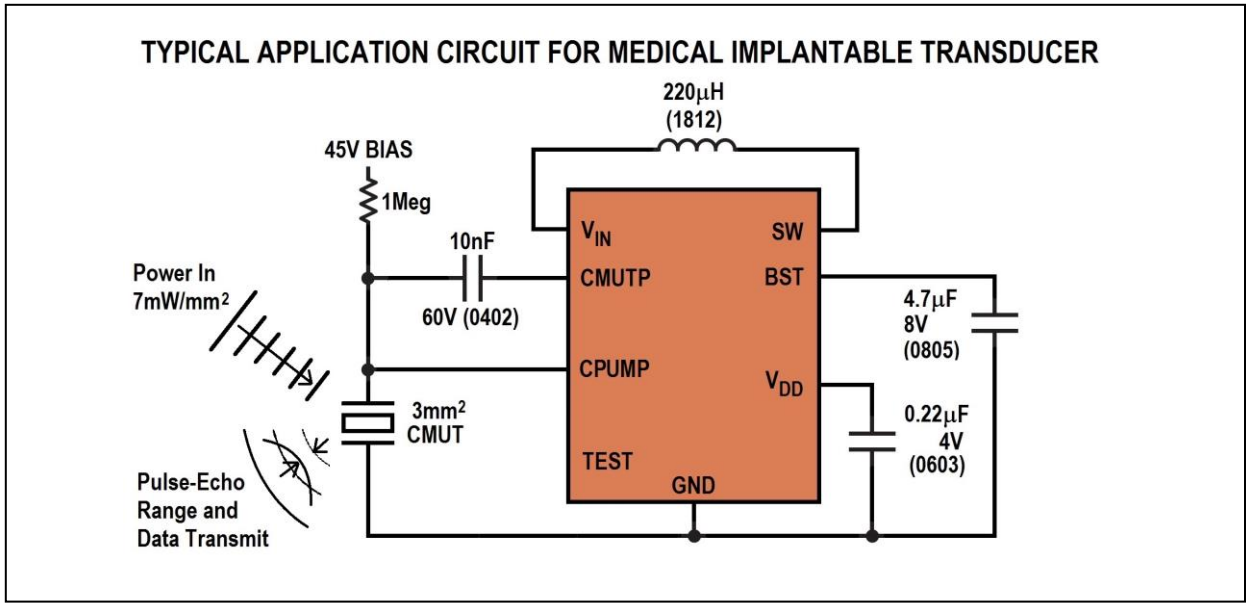

Figure 17. Application schematic for implantable EVAR monitoring device showing integrated circuit and external components, noting approximate device sizes . The 45V bias will be eliminated by pre-charging the CMUT.

Some of the key performance objectives are: **1)** charging a capacitor to 7V using ultrasonic energy at 7 mW/mm^2; **2)** automatically switching from charge mode to data logging mode; **3)** providing pulse-echo distance measurement up to 50mm (65μs); **4)** transmitting several bytes of data by bi-phasic pulse encoding scheme after each measurement, with up to 30 measurements per second; **5)** conserving charge on the power reservior to stretch the interval between charging events - when not in measure or transmit mode (200μs), reducing the quiescent current to 2μA; **6)** indicating low charge to external device by a unique data transmit code – and this code can also assist the external unit in locating the mote and focusing the acoustic energy. A functional block diagram of the integrated circuit is shown in Appendix A.

6.2 Process Selection

The plan is to fabricate the IC portion of the ultrasonic mote using Taiwan Semiconductor Manufacturing Corp (TSMC) 0.18 BCD Gen II process. With the small device sizes, the IC implementation is expected to be about 1 mm squared. This technology is an optimal choice because it has the bipolar (NPN and PNP) devices needed for the passive switching needed to rectify the input signal. It also has high voltage mosfet devices needed for the boost converter, and for the multi-stage chargepump needed to backbias the CMUT. Finally, the 0.18μm is a good choice for the dense logic and low quiescent current for high speed analog to digital conversion, timers and ultrasonic pulse controls.

6.3 Schematic Designs and Representative Waveforms

The charge-pump input to the power stage serves several purposes. First it rectifies the voltage from the CMUT during the push phase when the dielectric gap narrows. The charge pushed out of the CMUT drives the inductive based buck-boost power converter during the charging mode of operation. Second, it replenishes the charge on the coupling capacitor (or

CMUT) when the CMUT is in its pull phase when the gap widens and the CMUT output voltage sinks below GND. Third, and very importantly because this same CMUT is used as a driver-receiver for pulse-echo range measurement and data transmission during the active mode of device operation, the rectifier input can be programmed to be high impedance, neither sinking or sourcing current. The rectifier also must draw no current when the overall device is in an idle state – that is neither receiving power and not making a measurement or transmitting the data. It has been shown in the experiments that a bipolar PNP based pass device provides rectification with minimal collector-emitter voltage drop and minimal reverse current flow. The figure

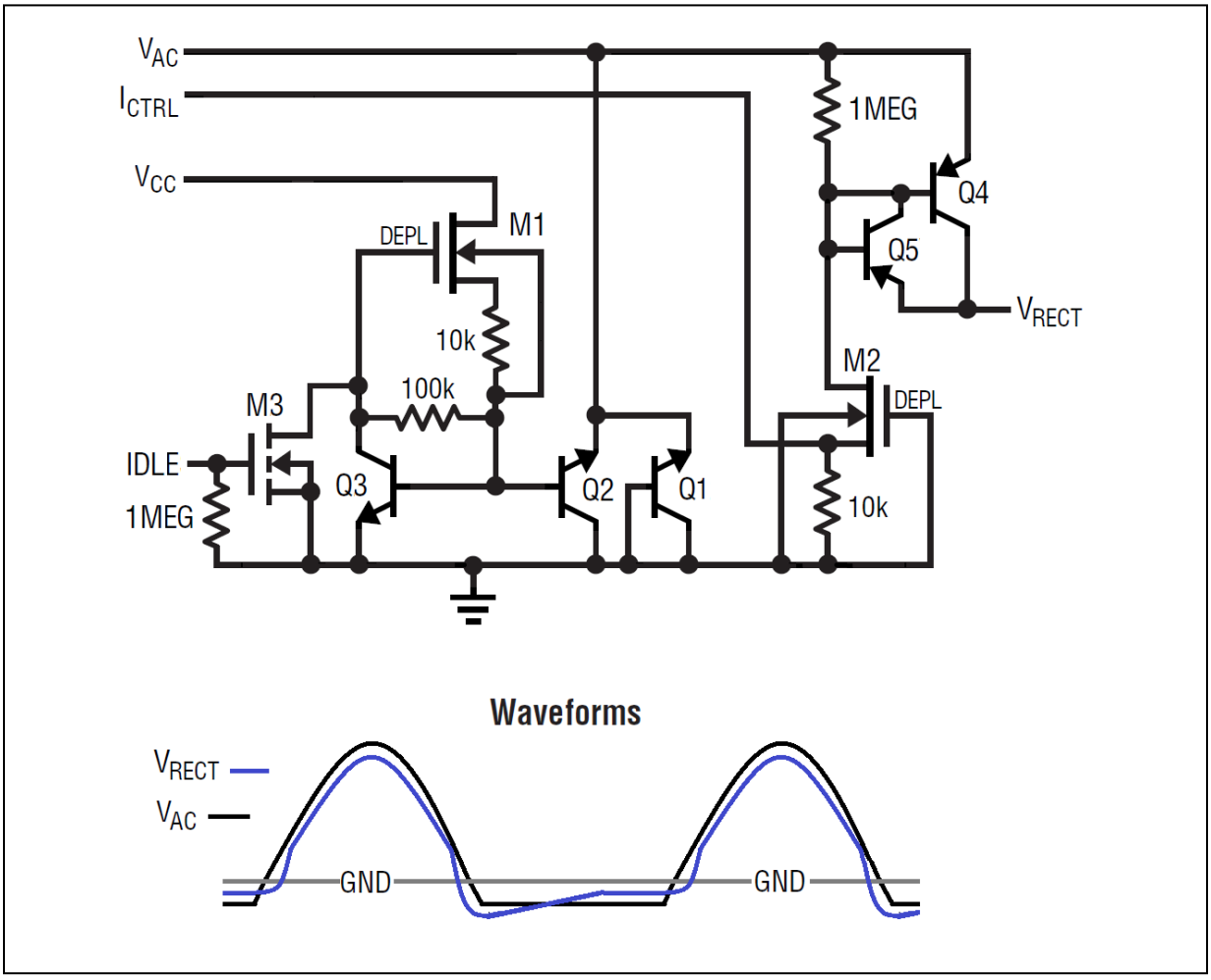

Figure 18. Chargepump rectifier for interface between buck-boost converter and CMUT. Bottom panel shows waveforms of AC signal from CMUT and rectified signal input to buck-boost power stage.

shows an integrated circuit implementation that is self-biasing, and can be put into a state where the V_{AC} input becomes high impedance when I_{CTRL} is sourcing current, and IDLE signal is high (~1V), turning on M3. Furthermore, when the IDLE signal is high, the current draw from VCC is reduced to less than 3μA. The operation of this circuit is as follows: 1) when V_{AC} is higher than V_{RECT} and >V_{BE} (0.6V) above GND, the device Q4 will turn on responding to base current supplied by depletion nmos M2. When the V_{RECT} is within a V_{SAT} ~50mV of V_{AC}, the device Q5 will shunt output current to the base to regulate the amount of base charge. Regulation is important because excess base change could slow the turnoff of Q4 when the voltage across the device reverses in the next phase of operation; 2) when V_{AC} falls below V_{RECT} and V_{AC} < GND, the device Q4 will turn off (quickly) and device Q2 will turn on responding to base current supplied by depletion nmos M1 from V_{CC}. Prior to V_{CC} being charged device Q1 will clamp V_{AC} to V_{BE} (0.6V) below GND. Device Q3 regulates the gate of M1 to provide the appropriate amount of base current to device Q2. Bipolar devices are important to the operation of this circuit for three reasons: first they operate at very low forward voltages compared with MOSFET threshold voltages; second, they have very high current gain with small changes in base-emitter voltage; and third, by construction their current gain is very asymmetric with the forward path having much higher current gain than the reverse path. These key attributes result in low voltage drops when passing current, a high degree of rectification on voltage reversal, and self-biasing at low supply voltage.

The voltage rectifier for the Vcc power supply used to power the bandgap and buck-boost control circuitry from a reservoir capacitor is quite different from the input rectifier. It performs as a peak voltage rectifier, so it can be a little simpler and biased actively (not passively), and with less current. There are two versions of this one, one for passing current from V_{RECT} (V_{IN}) to

V_{CC}, and the other for passing current from GND to V_{RECT} (V_{IN}) to supply the inductor when it discharges to the boosted output. The operation of the "V_{CC} Rectifier" circuit can be understood

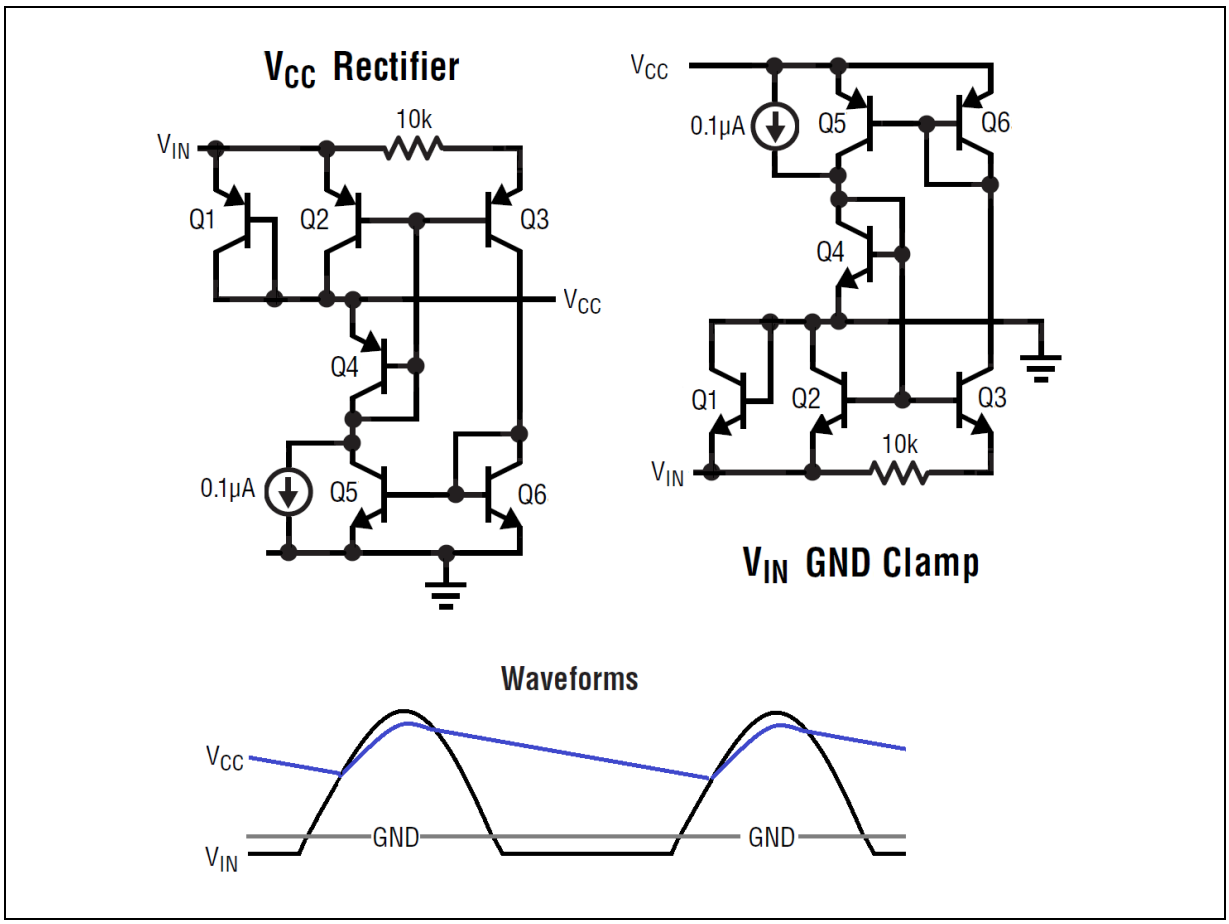

Figure 19. Schematics of low drop active Vcc rectifier and GND clamp circuits. Vcc rectifier captures peak of Vin waveform and provides power for IC startup. Vin ground clamp provides current to inductor during free-wheeling phase of buck-boost converter.

from the diagram. When V_{IN} exceeds V_{CC}, PNP devices Q2 and Q3 turn on. Q3 supplies additional base drive to Q2 through the current mirror Q5/Q6 so that just enough current is provided so that the collector-emitter drop across Q2 is less than 100mV. The "V_{IN} GND Clamp" circuit operation is basically the same as the "V_{CC} Rectifier" except the roles of NPNs and PNPs are reversed, so that the drop between VIN and GND is minimized when the inductor is pulling current from GND. These same circuits can used in other places such as the buck-boost output between SW and VBST, or in the Cockroft-Walton chargepump.

The Cockroft-Walton chargepump, having the output pin CPUMP in the application diagram of Figure 17, is used to increase the CMUT bias after startup. Using the initial bias from the embedded pre-charge as working capital, the chargepump adds bias charge to the 60V, 10nF coupling capacitor which boosts the output power capability. This charge is preserved during measuring modes by eliminating all bias and leakage currents from the CPUMP pin. The chargepump should be regulated to prevent output voltage overshoot forcing the CMUT into collapse mode. While the regulation algorithm is not yet determined, various control handles are apparent such as loading the chargepump with a current and increasing the drop across the rectifiers. Ideally, the regulation will eliminate manufacturing process variation from the embedded precharge. The 5pF output and input capacitors have to be rated for 25V.

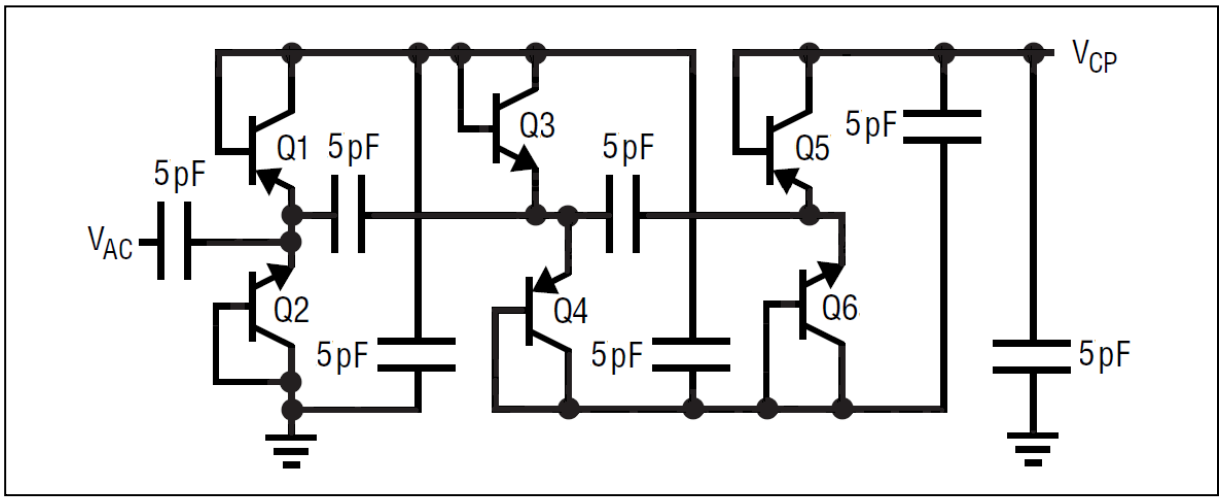

Figure 20. Schematic of Cockroft-Walton chargepump which has functions to augment the embedded CMUT bias charge to optimize power conversion. The chargepump input (Vac) and output (Vcp or CPUMP) straddle the 10nF coupling capacitor from the CMUT. Bipolar devices are representative of active rectifiers that reduce drops.

The buck-boost converter consists of the Vin ground clamp, the inductor, the switch and the output rectifier. The active versions of the ground clamp and output rectifier are shown in figure 19. This type of converter is capable of taking an input which varies both below and above the desired output and regulating a constant output voltage or charging a large capacitor. For this application and the CMUT source, the peak amount of current flowing in the inductor is

typically 10 mA or less, and the inductor current is expected to return to zero each cycle after discharging to the output, also known as discontinuous conduction mode (DCM). A high inductance, greater than 200 μH, is selected to store the maximum amount of energy while satisfying DCM at the ultrasound frequency of ~1 MHz. Because of the high inductor value and targeted small component size, a high series resistance is expected and tolerated given the low currents. The mosfet switch connecting the inductor to GND during the charging phase can be relatively high resistance also, up to 10 Ohm, with drain-source voltage capability less than 10V. The switch is operated between the charge and discharge phases based on the input voltage. The figure shows the expected waveforms during the buck-boost cycle. The switch is "on" during the inductor current ramp-up phase when the buck-boost input Vrect is high. When Vrect falls below ground because the CMUT pulls back and the input charge-pump replenishes the coupling capacitor, the switch turns off and the inductor current discharges to the output as seen by the Vsw voltage increasing and the inductor current decreasing.

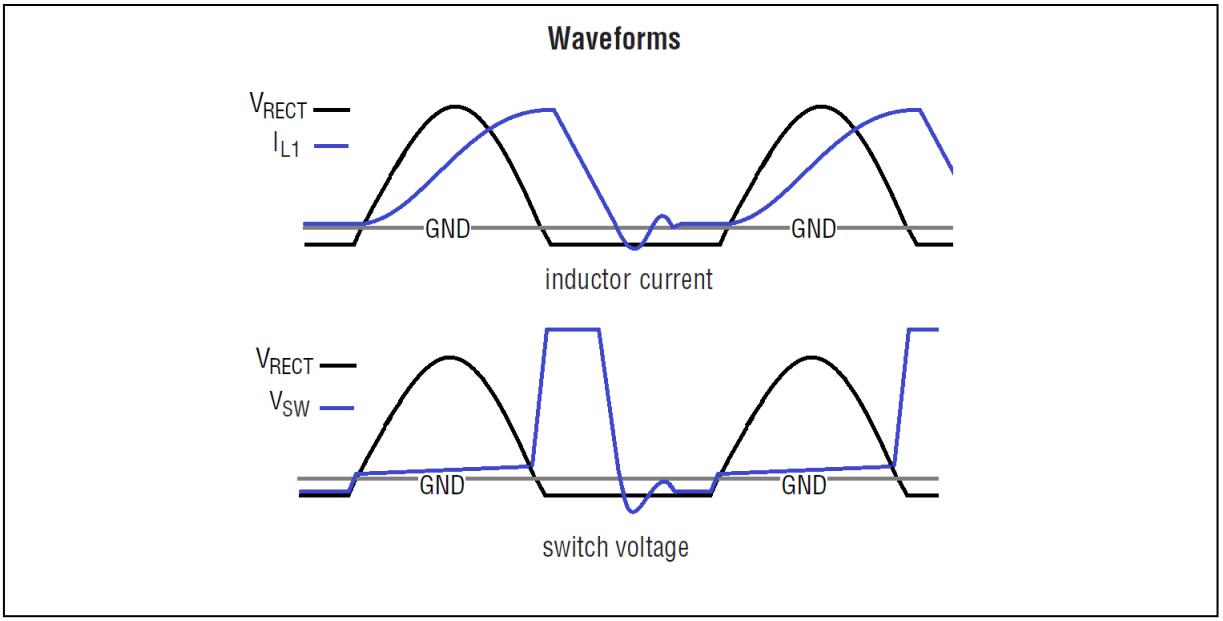

Figure 21. Current and voltage waveforms for the buck-boost converter.

CHAPTER 7. Conclusions

7.1 Thesis Summary

This thesis described the laboratory proofs-of-concept for a wireless implantable device that uses ultrasound for three functions: power delivery, communication and measurement of distance across an endovascular aneurysm repair stent-graft. We demonstrated key concepts for an implantable intravascular ultrasound device to monitor/diagnose endoleak in endovascular aneurysm repair stent-grafts. In benchtop studies using externally biased CMUTs and off-the-shelf discrete components, we demonstrated:

- Greater than 1 mW power recovery from a 3 mm^2 device with incident ultrasound intensity of 5 mW/mm^2, which is less than the ISPTA limit of 7.2 mW/mm^2.
- Ultrasonic biphasic communication concept with potential for high data rate
- Pulse-echo ranging from sensor to EVAR structures

The key findings of these studies justified the time and effort diverted from integrated circuit development. From these studies it is learned:

1. For power, a full-wave rectifier between the CMUT and the power converter is not needed and perhaps not desirable. During the negative half-cycle when the inductor current flows to the output, the input coupling capacitor is recharging for the next positive half-cycle. In this interval, the inductor current returns to zero, and this uniform starting point makes the control and stability of the buck-boost converter over a wide output range much simpler to implement. Also, having a hard-wired common ground between the CMUT and the IC makes the job of transmitting pulses and amplifying received signals much easier and less prone to ground offsets and noise.

2. For communication, while biphasic pulse signaling works, a balanced biphasic square pulse similar to what is generated by the commercial protocol device is not the optimal signal for driving the CMUT. The most balanced biphasic ultrasound pulse is generated by driving the CMUT with a sinusoidal pulse of pure frequency with a small phase offset. Simple to design electronics can get very close to this objective by emitting biphasic triangular pulses with unequal positive and negative lobes.
3. For measurement, the pulse echo return from the EVAR structure contains complex information, and as many as 4096 bits are needed to transmit this information. The original plan was to envelope detect this signal, discriminate the peak(s) and transmit the time stamp of a peak as the data for analysis by the external unit. While this method may be adequate, it could be better to include in the design a data converter to record the waveform, and dedicated on-board signal processing hardware to convert the waveform data to frequency domain. In frequency domain there are compression algorithms that can be employed to reduce the number of bits for transmission to the external unit where the waveform can be analyzed more thoroughly.

These observations impacting the integrated circuit design would not have been possible without the preliminary bench studies.

The second chapter provided the background information illuminating motivations for use of ultrasound and the CMUT in this application. The primary motivations for the use of ultrasound are 1) the long ranges that ultrasonic energy propagates in tissue; and 2) the ability to focus that energy to mm-scale devices, enabling communications and wireless power. The use of the CMUT provides advantages in manufacturability and integration with electronics, and the wide frequency bandwidth is needed for the biphasic pulsed communication strategy that

conserves energy. The third chapter presents the design approach used to receive acoustic power and convert it to electrical power for charging a reservoir capacitor, and the reasons for selecting a chargepump rectifier followed by a inductor based buck-boost. The results of the power converter demonstration using commercial off-the-shelf components and the steady improvement, eventually generating 1.1mW from 15mW incident acoustic power, compel further exploration using an integrated circuit design where the parasitic elements and loss mechanisms that reduce conversion efficiency can be minimized. The fourth chapter describes the considerations for wireless communications uplink and the approach selected, along with experimental setup diagrams and results from the laboratory proofs-of-concept. The fifth chapter expands on the clinical applications of the deep implantable device: namely endoleak monitoring and cardiac stem cell patch ingraft monitoring. The sixth chapter provides a plan for the integrated circuit (IC) implementation, some key circuit schematics with explanations of their operation, and a description of the preferred process technology for implementing this IC.

7.2 Future Work

The IC will have to be designed (schematic and physical layout) and simulated, manufactured, and tested for parametric performance. Once the performance is verified, the IC can be mounted and connected by bondwires on a board to the other components (CMUT, inductor, capacitor). This board assembly will have to be tested for functionality in and out of acoustic medium (oil). The functional tests include power conversion from acoustic energy, signaling, measurements and encoding of data. None of these require development of an external unit: the power can be provided to the circuit externally for checking the measurement and uplink functions. For the power conversion testing, a passive load such as an LED can be

used to demonstrate efficiency. One priority item to investigate is to measure the effect of angle of incidence upon power conversion ratio.

The CMUT devices have a fundamental need for a voltage bias in order to operate as a power receiver. In this work, for these particular CMUTs, we used a bias varying from 30V to 50V. The need for this voltage supply is in conflict with the idea of a remote device as being self-biased ready to generate electric power upon receipt of ultrasonic energy. One solution of this problem is to have a battery or capacitor always charged and biasing the CMUT, and never allowing voltage to drop below a minimum threshold. However, this minimum voltage requirement could impact the device's lifetime and perceived reliability. A better approach is to

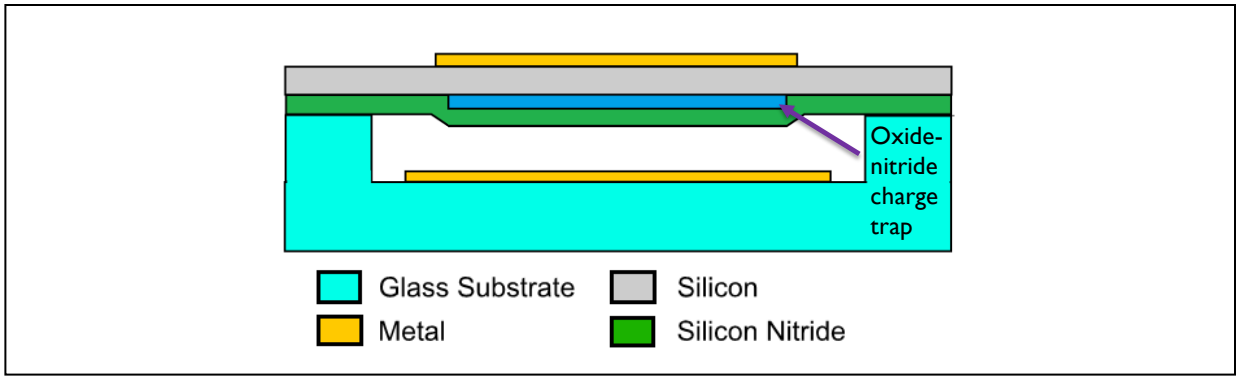

Figure 22. Cross section of CMUT with charge pre-bias capability.

use the "electret" concept to bias the capacitive membrane with a predetermined fixed charge that could not leak off. CMUT devices with a silicon membrane typically use silicon nitride as a dielectric layer to prevent shorting of the membrane to the bottom electrode in a collapse event. A manufacturing performance issue with this material selection has been that the trapped charge in the silicon nitride causes CMUTs to have variation in the pre-bias so that their gain and signal strength as an ultrasonic transducer has an element of randomness. In imaging applications, the elimination of pre-bias is desirable for device uniformity and matching. For the case of a power transducer, the trapped charge could be a key feature provided it can be well enough controlled. The literature reports electrets composed of a silicon-oxide/ silicon-nitride stack, charged to

100V with a corona discharge which hold their charge over long periods of time and at high temperatures [28]. It would be worth evaluating a CMUT with the electret (shown in green in the figure) deposited on the membrane facing the bottom electrode, and precharged before anodic bonding.

Eventually, to proceed with in vitro and in vivo studies will require development of the external unit which sends the ultrasonic power and receives the data. Once the implantable is mounted to the EVAR device, or in configuration with the EVAR, it will be necessary to calibrate the measurements in the presence and absence of endoleak to show the clinical significance of the distance measurements, since this particular metric has not been used previously. It is likely that a series of measurements will be needed during a cardiac interval to measure the elastic response of the implant to pulse pressure variation. In the presence of endoleak, blood pressure will be equalized on both sides of the stent/graft, and this should reduce the variation in distance over the cardiac interval compared with no endoleak.

In the long term, the use of such a device will depend upon acceptance by the medical profession. The alternative of annual invasive followup just to screen for EVAR endoleak is costly to the patient and the medical reimbursement system, and wastes physician time and limited hospital resources. The use of a dedicated handheld ultrasonic device to power the implantable and read its data in the outpatient setting is made practical by the pioneering development of lower cost ultrasound technology based on the CMUT by such companies as Butterfly Network, and this development is likely to be followed very soon by the much larger healthcare equipment manufacturers. The acceptance of an implantable as a diagnostic device is probably much easier than the path of a therapy device. The acceptance of this device requires that the sensitivity or probability of detection of endoleak is very high so that there is little

chance that a valid condition will be missed; while the specificity is also high enough so there is minimal waste of interventional resources from false positives for the endoleak condition. If both these conditions, sensitivity and specificity, are satisfied in the new device the reduction in cost of follow-up, and improvement to patient comfort and compliance with annual checks will hasten its adoption.

REFERENCES

[1] M. Roes, J. Duarte, E. Lomonova and M. Hendrix, "Acoustic Energy Transfer: A Review," *IEEE Transactions on Industrial Electronics,* vol. 60, no. 1, pp. 242-248, JANUARY 2013.

[2] A. Denisov and E. Yeatman, "Ultrasonic vs. Inductive Power Delivery for Miniature Biomedical Implants," in *International Conference on Body Sensor Networks,* Singapore, 2010.

[3] H. Basaeri, D. Christensen and S. Roundy, "A review of acoustic power transfer for bio-medical implants," *Smart Materials and Structures,* vol. 25, no. 12, 2016.

[4] K. Petersen, "Silicon as a Mechanical Material," *Proceedings of the IEEE,* vol. 70, no. 5, pp. 420-457, 1982.

[5] X. Jin, I. Ladabaum and B. Khuri-Yakub, "The microfabrication of capacitive ultrasonic transducers," *IEEE/ASME J. Microelectromech. Syst.,* vol. 7, p. 295–302, 1998.

[6] G. Moore, "Cramming more components onto integrated circuits," *Electronics,* vol. 38, no. 8, pp. 1-6, 1965.

[7] Europractice IC Service, "MPW & MINI@SIC," [Online]. Available: https://europractice-ic.com/mpw-prototyping/general/mpw-minisic/. [Accessed 13 March 2020].

[8] Riley, Rick, "EBR-Systems-Announces-Human-Implants-WiCS," EBR-Systems, 1 May 2011. [Online]. Available: https://www.businesswire.com/news/home/20110503005771/en/EBR-Systems-Announces-Human-Implants-WiCS. [Accessed 8 Nov 2018].

[9] R. Sanders, "Sprinkling of neural dust opens door to electroceuticals | Berkeley News," 3 August 2016. [Online]. Available: http://news.berkeley.edu/2016/08/03/sprinkling-of-neural-dust-opens-door-to-electroceuticals/.

[10] D. Seo, "PhD Thesis - Design of Ultrasonic Power Link for Neural Dust," UC Berkeley, Berkeley, 2016.

[11] A. Dua and e. al, "Epidemiology of aortic aneurysm repair in the United States from 2000 to 2010," *Journal of Vascular Surgery,* vol. 59, no. 6, p. 1512–1517, 2014.

[12] J. Golzarian, E. Maes and S. Sun, "Endoleak: Treatment Options," *Techniques in Vascular and Interventional Radiology,* vol. 8, no. 1, pp. 41-49, 2005.

[13] M. Daniele, "Centre to Centre Proposal, EchoSense," NSF-NERC ASSIST / CÚRAM / CCRCB, NC State University, 2018.

[14] T. Su, et. al., "Cardiac Stem Cell Patch Integrated with Microengineered Blood Vessels Promotes Cardiomyocyte Proliferation and Neovascularization after Acute Myocardial Infarction," *ACS Appl. Mater. Interfaces,* vol. 10, p. 33088−33096, 2018.

[15] M.C. Ho, et. al., "Long-term measurement results of pre-charged CMUTs with zero external bias operation," in *IEEE IUS*, Dresden, Germany, 2012.

[16] K.K. Park, et. al, "Zero-bias resonant sensor with an oxide-nitride layer as charge trap," in *IEEE Sensors*, Waikoloa, Hawaii, 2010.

[17] A. Kshirsagar, et. al., "Pre-charged CMUTs with efficient low-bias voltage operation for medical applications," in *IEEE IUS*, Prague, Czech Republic, 2013.

[18] X. Xie, L. Rieth, R. Caldwell, M. Diwekar, P. Tathireddy, R. Sharma and F. Solzbacher, "Long-Term Bilayer Encapsulation Performance of Atomic Layer Deposited Al2O3 and Parylene C for Biomedical Implantable Devices," *IEEE Transactions on Biomedical Engineering*, vol. 60, no. 10, pp. 2943-2951, 2013.

[19] J. Bamber, "Ch. 4 "Attenuation and Absorption"," in *Physical Principles of Medical Ultrasonics*, Chichester, UK, Wiley, 2004, pp. 118-199.

[20] R. Cobbold, "Ch. 1 "Introduction"," in *Foundations of Biomedical Ultrasound*, New York, NY, Oxford University Press, 2007, pp. 3-95.

[21] Q. Chen and G. Thouas, Biomaterials: A Basic Introduction, Boca Raton, FL: CRC Press, 2015.

[22] A. Lohfink and P. Eccardt, "Linear and Nonlinear Equivalent Circuit Modeling of CMUTs," *IEEE Transactions on Ultrasonics, Ferroelectrics, and Frequency Control*, vol. 52, no. 12, pp. 2163-2172, 2005.

[23] G. G. Yaralioglu, M. H. Badi, A. S. Ergun and B. T. Khuri-Yakub, "Improved equivalent circuit and finite element method modeling of capacitive micromachined ultrasonic transducers," in *Proceedings IEEE Ultrasonics Symposium*, Honolulu, Hawaii, 2003.

[24] F. Yalcin Yamaner, X. Zhang and Ö. Oralkan, "Fabrication of Anodically Bonded Capacitive Micromachined Ultrasonic Transducers with Vacuum-Sealed Cavities," in *IEEE International Ultrasonics Symposium Proceedings*, Chicago, IL, 2014.

[25] O. Adelegan and e. al., "A 2D Capacitive Micromachined Ultrasonic Transducer (CMUT) Array with Through-Glass-Via Interconnects Fabricated Using Sacrificial Etching Process," in *IEEE Ultrasonics Symposium*, Glasgow, UK, 2019.

[26] J. Charthad, T. C. Chang, Z. Liu, A. Sawaby, M. Weber and A. Arbabian, "A mm-Sized Wireless Implantable Device for Electrical Stimulation of Peripheral Nerves," *IEEE Transactions on Biomedical Circuits and Systems*, vol. 12, no. 2, pp. 257-270, 2018.

[27] Analog Devices, Inc, *Datasheet, LTC6820 isoSPI Isolated Communications Interface*, 2018.

[28] V. Leonov, P. Fiorini and C. V. Hoof, "Rapid corona charging and stability of positive charge stored in SiO2/Si3N4 electrets," in *12th International Symposium on Electrets*, 2005.

[29] J. M. Douglass, "Isolated Communications Interface". US Patent 8,908,779, 9 December 2014.

APPENDICES

Appendix A

Functional Block Diagram of IC and Pin Descriptions Table

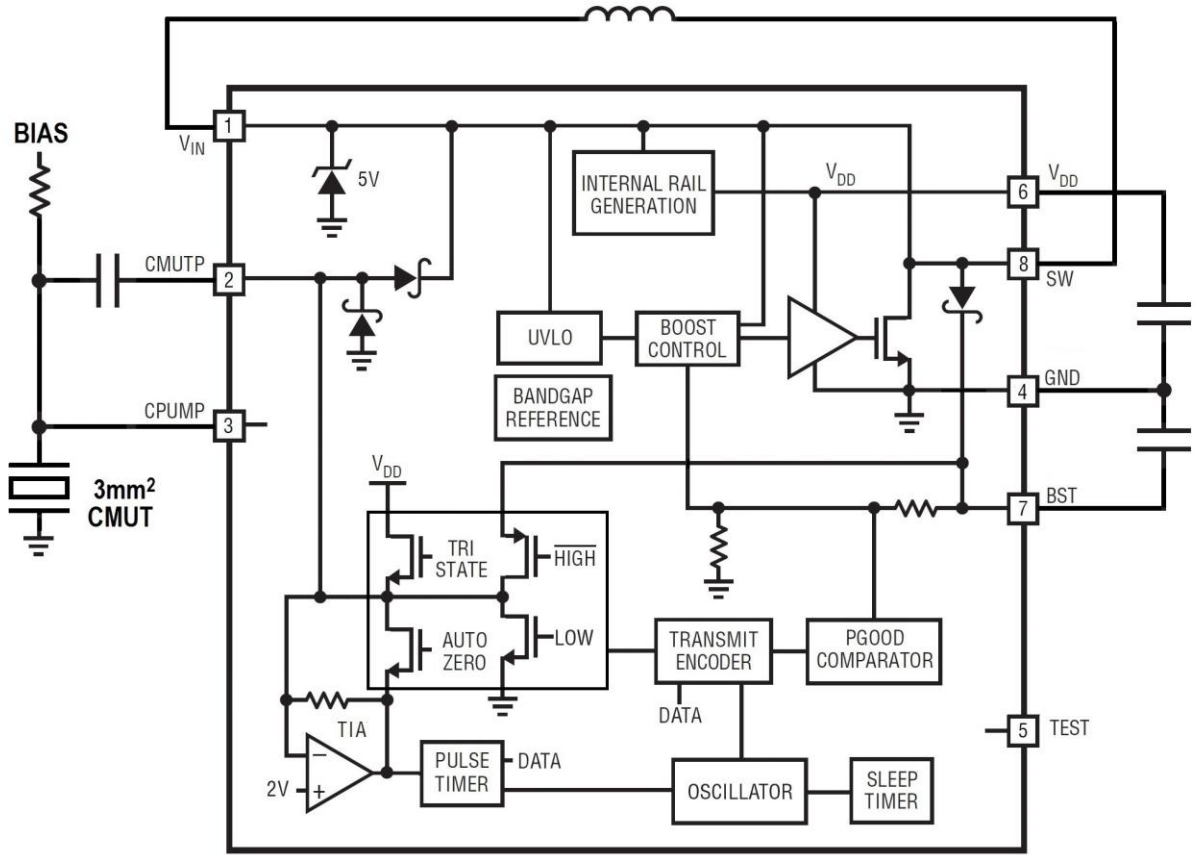

VIN (Pin 1): Output of Full-Wave Rectifier from CMUT. Input to inductive boost converter, and startup source for VDD until LDO achieves regulation. Do not load this pin with an external capacitor because the voltage on this pin controls the phase of the boost converter.

CMUTP (Pin 2): Positive Node of CMUT. Typically the buried metal (cavity) electrode. For a non-electret CMUT this node should be connected to the filter cap which goes to the bias-T. Input to full-wave rectifier and receive mode transimpedance amplifier, output of 3-level transmit driver.

CPUMP (Pin 3): Chargepump boosted output to bias the CMUT on the other side of the capacitor. Boosts to 4x amplitude of CMUTP. Some intrinsic charge on the CMUT is assumed, needed for startup

GND (Pin 4): Ground. Connect external capacitors to this terminal, and common (reference) terminal of CMUT.

TEST (Pin 5): Test pin. Three level logic input pin. Tie to GND during normal operation. Drive TEST above VDD with 0.1mA to enter test mode, below VDD/2 then above VDD to clock test modes. Drive VDD below UVLO~2.2V to clock test modes. Drive VDD below UVLO~2.2V to exit or reset test mode. As an input, TEST forces the biphasic communication pulses on the transmitter in the two frequencies, long or short, and with both polarities. As an output pin: TEST reports the internal clock in both modes (SLEEP or Active), the threshold for high/low gate of the ultrasonic return pulse at a particular time elapsed set by the test mode selection, and the direct output of the TIA. Test modes override the maximum on-time for SW.

V_{DD} (Pin 6): LDO Regulated Supply for chip loads including amplifiers, comparators and logic. The LDO supply is BST after startup is complete and while BST>VDD>2.5V. Regulates to the greater value of BST/2 or 3V.

BST (Pin 7): Boost Regulator Output. Regulates to 7.5V when ultrasonic energy is provided. Flags undervoltage when BST drops below 6V.

SW (Pin 8): Switching node of boost converter. Switch is on for a maximum time of ~1µs when Vin>0.5V, Vdd>2.2V, Isw<10mA and BST<7.5V.